

Boson-fermion pairing and condensation in two-dimensional Bose-Fermi mixtures

Leonardo Pisani,^{1,2} Pietro Bovini,^{1,2} Fabrizio Pavan,³ and Pierbiagio Pieri^{1,2}

¹*Dipartimento di Fisica e Astronomia “Augusto Righi”,
Università di Bologna, Via Irnerio 46, I-40126, Bologna, Italy*

²*INFN, Sezione di Bologna, Viale Berti Pichat 6/2, I-40127, Bologna, Italy*

³*Dipartimento di Fisica E. Pancini - Università di Napoli Federico II - I-80126 Napoli, Italy*

We consider a mixture of bosons and spin-polarized fermions in two dimensions at zero temperature with a tunable Bose-Fermi attraction. By adopting a diagrammatic T -matrix approach, we analyze the behavior of several thermodynamic quantities for the two species as a function of the density ratio and coupling strength, including the chemical potentials, the momentum distribution functions, the boson condensate density, and the Tan’s contact parameter. By increasing the Bose-Fermi attraction, we find that the condensate is progressively depleted and Bose-Fermi pairs form, with a small fraction of condensed bosons surviving even for strong Bose-Fermi attraction. This small condensate proves sufficient to hybridize molecular and atomic states, producing quasi-particles with unusual Fermi liquid features. A nearly universal behavior of the condensate fraction, the bosonic momentum distribution, and Tan’s contact parameter with respect to the density ratio is also found.

I. INTRODUCTION

Mixed systems of bosons and fermions are at the base of our understanding of the physical world. They feature in the Standard Model of elementary-particle physics as gauge and matter fields, respectively, in high density quark matter as diquarks interacting with unpaired quarks [1], in nuclear matter in the interacting boson-fermion model for atomic nuclei with an odd number of protons or neutrons [2], and as boson-mediated interactions in soft [3] as well as condensed [4] matter. Ultra-cold atomic gases provide an exceptionally versatile platform for the simulation of quantum matter [5]. In the case of Bose-Fermi (BF) atomic mixtures, several realizations [6–39] have permitted to explore a wide range of phenomena like phase separation [22], polarons [13, 17, 23, 26, 31], dual superfluidity [15, 16, 19, 20], collective excitations [34, 35], mediated interactions [28, 36–38], and Feshbach molecules [6, 8, 10, 25, 30, 33]

In a parallel fashion, BF mixtures have also been realized in optical semiconductor micro-cavities [40–42] thanks to the recent advent of atomically thin transition metal dichalcogenides [43, 44]. These materials intrinsically offer a remarkable opportunity to investigate the physics in two dimensions (2D) where topological phases play a crucial role [45, 46].

However, the unique flexibility of atomic gases is unrivaled when the need arises to manipulate dimensionality and interaction strength at the same time. Confinement induced resonances accomplish this purpose by allowing for the realization of a dimensional crossover, starting from 3D confinement down to (quasi-)2D one. If the energy level spacing of the 3D trapping system (or equivalently the confinement length) is kept much larger than the energy (shorter than the length) scales of the intervening scattering processes, the system becomes effectively 2D and the ensuing 2D scattering length can be manipulated by varying either the scattering length associated to the original 3D Feshbach resonance and/or the confinement length, yet ensuring the quasi-2D condition above remains satisfied [47–49]. This situation is particularly apt for BF mixtures, for which one would need to adjust independently the BF and the boson-boson (BB) interactions owing

to the mechanical stability of the assembly being conditioned primarily by that of the Bose component [50]. Having at one’s disposal two independent degrees of freedom in the 3D scattering length and in the confinement length, one can then correspondingly tune the effective BF and BB interactions (even though in a highly non-linear fashion [47]) and simultaneously analyze the stability of different phases of the mixture across the whole resonant regime.

Under such circumstances, a recent work has shown that two-dimensional weakly bound fermionic molecules formed in a BF mixture with attractive BF and repulsive BB interactions are expected to be collisionally stable and should exhibit a strong p-wave mutual attraction [51]. In fact three-body recombination, which has historically plagued these mixed systems in three dimensions, is concomitantly avoided because Efimovian processes are suppressed in 2D.

P -wave superfluidity is intensely pursued in both atomic based [52] and semiconductor based [45, 53] mixtures, as it opens the way to the exploration of topologically protected states, including Majorana modes and non-Abelian vortex excitations [54, 55], hence offering a route for the implementation of fault-tolerant quantum computation [56–61].

Under the above scenario, it is crucial to explore BF mixtures with a tunable BF attraction in a 2D setting. Until now, theoretical efforts have concentrated mainly on 3D settings [62–83]. In 2D, theoretical work has been sparse so far [84–87] and has primarily dealt with phase competition in optical lattices [84, 86], phase stability in atomic traps [85], or with the bosonic impurity limit of a boson density n_B much smaller than the fermion density n_F [87].

In this work, we study a 2D BF mixture in homogeneous space with boson and fermion densities spanning from the bosonic impurity limit ($n_B \ll n_F$) to the matched density regime ($n_B = n_F$). Similarly to the analyses carried out in 3D [73, 77, 80, 81, 83, 88], we are here interested in the competition between boson condensation and BF pairing in mixtures with an attractive and tunable BF interaction at zero temperature. We focus on the case with concentration of bosons $x = n_B/n_F \leq 1$, such that a full competition between pairing and condensation is allowed. The BB interaction is considered to be repulsive for mechanical stability reasons.

Our main results are as follows. (i) We found that the condensate is progressively depleted as the BF attraction increases, in analogy with the 3D case. However, while in 3D the condensate vanishes beyond a critical coupling strength, in 2D the condensate does not exactly vanish but rather becomes exponentially small with the coupling strength. (ii) Similarly to the 3D case, we uncover a nearly universal behavior of the condensate fraction, the bosonic momentum distribution, and Tan's contact parameter with respect to the boson concentration. (iii) BF pairs form for sufficiently strong BF attraction. Quite generally, these composite fermions are hybridized states between a pure molecular bound state and an unpaired state made of a fermionic atom and a boson belonging to the condensate. We found that these hybridized states produce quasi-particles with rather peculiar Fermi liquid features. (iv) The boson momentum distribution function show quite a rich behavior when varying the BF coupling strength and boson concentration, which could in principle be tested in future experiments with BF mixtures.

The article is organized as follows. In Sec. II we introduce the model Hamiltonian, illustrate the diagrammatic theory of choice and lay out the full set of thermodynamic equations to solve. In Sec. III we explore the strong-coupling limit for the BF coupling parameter. In this limit, a set of semi-analytical and rather simple equations can be derived, allowing us to obtain crucial insights on the microscopic physics and phenomenology of a strongly attractive BF mixture in 2D. In Sec. IV we present our numerical results for the boson and fermion momentum distributions, corresponding chemical potentials, condensate density and Tan's contact parameter. In Sec. V we discuss virtues and limitations of our approach and outline perspectives for future work.

II. FORMALISM

A. The system Hamiltonian

We consider a mixture of bosons (B) and single-component fermions (F) with interspecies attraction in a two-dimensional homogeneous setting, and focus on the zero temperature limit in which bosons may condense even in 2D [89].

The system is assumed to be dilute such that the range of all interactions is smaller than the average inter-particle distance. Most common regimes of current experiments on BF mixtures involve the presence of a broad Fano-Feshbach resonance, whereby the boson-fermion scattering length is larger than the interaction range. This justifies the adoption of an effective pseudo-potential of the point-contact form [90] as far as the modeling of the BF interaction is concerned. The BB interaction is assumed to be short-ranged and weakly repulsive in order to make the system mechanically stable. Hence, within a minimal model approach, the resulting Hamiltonian

in the grand-canonical ensemble has the form

$$\begin{aligned}
 H = & \sum_{s=B,F} \int d\mathbf{r} \psi_s^\dagger(\mathbf{r}) \left(-\frac{\nabla^2}{2m_s} - \mu_s \right) \psi_s(\mathbf{r}) \\
 & + v_0^{\text{BF}} \int d\mathbf{r} \psi_B^\dagger(\mathbf{r}) \psi_F^\dagger(\mathbf{r}) \psi_F(\mathbf{r}) \psi_B(\mathbf{r}) \\
 & + \frac{1}{2} \int d\mathbf{r} \int d\mathbf{r}' \psi_B^\dagger(\mathbf{r}) \psi_B^\dagger(\mathbf{r}') U_{\text{BB}}(\mathbf{r} - \mathbf{r}') \psi_B(\mathbf{r}') \psi_B(\mathbf{r}),
 \end{aligned} \tag{1}$$

where ψ_s^\dagger and ψ_s respectively create and destroy a particle of mass m_s and chemical potential μ_s , with $s = B, F$ indicating the bosonic or fermionic nature. We consider two assemblies with densities $n_B \leq n_F$, relative concentration $x = n_B/n_F$ and equal masses $m_B = m_F$ and adopt the convention $\hbar = k_B = 1$ throughout this paper.

The first term in Eq. (1) describes a system of non-interacting single-component bosons and fermions. The second term accounts for the boson-fermion interaction, which is attractive with coupling strength v_0^{BF} . The third term deals with the boson-boson interaction, which is taken to be weakly repulsive for stability reasons and can be treated perturbatively at the level of the Bogoliubov approximation for the two-dimensional Bose gas (as developed originally by Schick [91]). This boils down to adopting the effective replacement $U(\mathbf{r} - \mathbf{r}') \rightarrow v_0^{\text{BB}} \delta(\mathbf{r} - \mathbf{r}')$ with an effective BB coupling strength $v_0^{\text{BB}} = 4\pi\eta_B/m_B$, where $\eta_B = -1/\ln(n_B a_{\text{BB}}^2)$ is the (small) gas parameter and a_{BB} is the (2D) BB scattering length. Finally, the s -wave fermion-fermion scattering is forbidden by Pauli exclusion principle ($v_0^{\text{FF}} = 0$).

The BF attractive contact interaction needs to be regularized by expressing the bare strength v_0^{BF} in terms of the scattering length a_{BF} . This is achieved by the equation

$$\frac{1}{v_0^{\text{BF}}} = - \int \frac{d\mathbf{k}}{(2\pi)^2} \frac{1}{\varepsilon_0 + \frac{k^2}{2m_r}}, \tag{2}$$

relating the bare coupling strength v_0^{BF} with the boson-fermion binding energy $\varepsilon_0 = 1/(2m_r a_{\text{BF}}^2)$ of the associated two-body problem in vacuum, where a_{BF} is the (2D) BF scattering length and $m_r = m_B m_F / (m_B + m_F)$ is the reduced mass of the boson-fermion system. The ultraviolet-divergent integral on the right-hand side of Eq. (2) compensates analogous divergencies occurring in many-body diagrammatic perturbation theory.

In analogy with 2D fermionic systems, we introduce an effective boson-fermion coupling parameter $g = -\ln(k_F a_{\text{BF}})$, where $k_F = \sqrt{4\pi n_F}$ is the 2D Fermi momentum of a non-interacting Fermi gas with the same density n_F of the fermionic component. The weak and strong BF coupling regimes are defined by $g \ll -1$ and $g \gg 1$ but, in practice, they are well represented by the effective ranges, $g \lesssim -2$ and $g \gtrsim 2$, respectively.

Based on physical intuition, and in analogy with the 3D case, one expects the following picture when the BF coupling strength is varied. In the weak coupling limit, bosons are expected to be almost fully condensed (compatibly with a

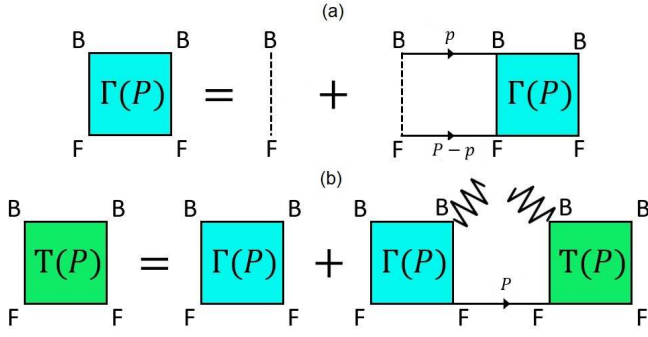


Figure 1. Feynman's diagrams for the T -matrix $\Gamma(P)$ in the normal phase (a) and $T(P)$ in the condensed phase (b). Full lines correspond to bare boson (B) and fermion (F) Green's functions, dashed lines to bare BF interactions and zigzag lines to condensate factors $\sqrt{n_0}$.

quantum depletion determined by η_B) and fermions to fill up a Fermi sphere with chemical potential renormalized at the mean-field level. In the strong coupling limit, bosons are instead expected to be expelled out of the condensate and form molecular fermions that fill up a Fermi sphere. We will discuss below to what extent this simple picture continues to hold also in two dimensions.

B. Many-body T -matrix

The diagrammatic many-body approach adopted in the present work relies on previous works on BF mixtures in 3D, both above [73] and below [88] the BEC transition temperature, based on the non-self-consistent T -matrix (ladder) approximation. In these works, the T -matrix approach was shown to recover the well-known polaron-molecule transition of an impurity in a polarized Fermi gas as the coupling strength is increased and to predict a universal behavior of the condensate fraction as a function of the coupling strength with respect to the boson concentration. Such outcomes were recently confirmed in a break-through experiment on 3D BF mixtures, where for the first time the regime of double degenerate BF mixtures with matching densities was reached [33]. There the authors observed the existence of a quantum critical point at the polaron-to-molecule phase transition and confirmed the universal character of the condensate fraction with respect to the boson concentration, predicted in [88] some time before. Based on these solid and sound results, we keep the same diagrammatic choice of [88] and extend it to the 2D case.

Let us first consider the normal phase, in which the condensate fraction n_0 is identically zero [73]. The boson-fermion interaction is captured by the series of repeated scattering events in the T -matrix $\Gamma(P)$ in Fig. 1(a), where continuous lines indicate bare fermionic or bosonic propagators, while dashed lines indicate the bare boson-fermion interaction v_0^{BF} .

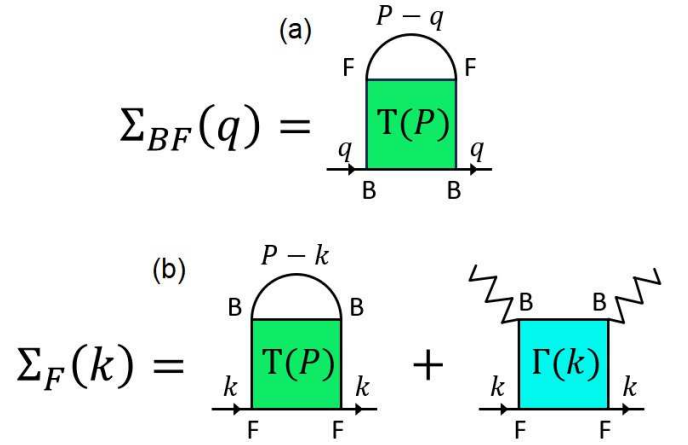


Figure 2. Feynman's diagrams for the boson self-energy Σ_{BF} arising from interactions with fermions (a) and fermion self-energy Σ_F (b). Full lines correspond to bare boson and fermion Green's functions, and zigzag lines to condensate factors $\sqrt{n_0}$.

In the zero temperature limit, Feynman rules yield

$$\Gamma(\mathbf{P}, \Omega) = v_0^{\text{BF}} - v_0^{\text{BF}} \Gamma(\mathbf{P}, \Omega) \times \int \frac{d\mathbf{p}}{(2\pi)^2} \int_{-\infty}^{\infty} \frac{d\omega}{2\pi} G_F^0(\mathbf{P} - \mathbf{p}, \Omega - \omega) G_B^0(\mathbf{p}, \omega) \quad (3)$$

with G_B^0 and G_F^0 the bare Green's functions for bosons and fermions

$$G_s^0(\mathbf{k}, \omega) = \frac{1}{i\omega - \xi_{\mathbf{k}}^s}, \quad s = \text{B, F}, \quad (4)$$

where $\xi_{\mathbf{k}}^s = k^2/2m_s - \mu_s$.

Following Appendix A, one obtains

$$\Gamma(\mathbf{P}, \Omega) = \frac{1}{T_2(\mathbf{P}, \Omega)^{-1} - I_F(\mathbf{P}, \Omega)}, \quad (5)$$

where T_2 is the off-shell two-body T -matrix in vacuum and the contribution $I_F(\mathbf{P}, \Omega)$ stems from the presence of the fermionic medium (see Appendix A for details). Note that the present diagrammatic approach corresponds to the zero-temperature limit of the Matsubara formalism at finite temperature. We will thus work on the imaginary frequency axis rather than on the real frequency one (as instead is standard practice at $T = 0$ [92]). This choice is particularly useful to avoid singularities of the Green's function on the real frequency axis.

We now consider the condensed phase, for which additional diagrams are to be taken into account [88]. These are shown in Fig. 1(b) with zigzag lines representing condensate factors: here additional fluctuation processes are introduced by allowing the BF pairs to break up and exchange bosons with the condensate. The resulting Bethe-Salpeter equation for the T -matrix in the condensed phase $T(\mathbf{P}, \Omega)$ thus reads

$$T(\mathbf{P}, \Omega) = \Gamma(\mathbf{P}, \Omega) + n_0 \Gamma(\mathbf{P}, \Omega) G_F^0(\mathbf{P}, \Omega) T(\mathbf{P}, \Omega), \quad (6)$$

which immediately yields

$$T(\mathbf{P}, \Omega) = \frac{1}{\Gamma(\mathbf{P}, \Omega)^{-1} - n_0 G_F^0(\mathbf{P}, \Omega)}. \quad (7)$$

Viewing $T(\mathbf{P}, \Omega)$ and $\Gamma(\mathbf{P}, \Omega)$ as dressed and undressed pair propagators respectively, the above equation can be interpreted as a Dyson's equation for the pair propagator $T(\mathbf{P}, \Omega)$, with the related self-energy insertion $n_0 G_F^0(\mathbf{P}, \Omega)$ representing the exchange of bosons with the condensate.

C. Boson and fermion self-energies

We now discuss the bosonic and fermionic self-energies within the present T -matrix approach.

The bosonic self-energy is made of two terms: the interaction with fermions and that with other bosons. The former is shown in Fig. 2(a), yielding the expression

$$\Sigma_{\text{BF}}(\mathbf{k}, \omega) = \int \frac{d\mathbf{P}}{(2\pi)^2} \int \frac{d\Omega}{2\pi} T(\mathbf{P}, \Omega) G_F^0(\mathbf{P} - \mathbf{k}, \Omega - \omega) e^{i\Omega 0^+}. \quad (8)$$

Note here that we adopt a sign convention such that the T -matrix $T(\mathbf{P}, \Omega)$ reduces to the T -matrix in vacuum [93].

To ensure the mechanical stability of the bosonic component of the mixture, a minimal repulsive interaction between bosons is needed. This repulsion is described within the standard Bogoliubov approximation for weakly interacting bosons [94]. Extension of the latter to two dimensions was originally done by Schick in [91] (and later by Popov [95]), who showed that the lowest order anomalous and normal self-energies have the form

$$\Sigma_{12} = \frac{-4\pi n_0}{m_B \ln(n_B a_{\text{BB}}^2)}, \quad \Sigma_{11} = 2\Sigma_{12}, \quad (9)$$

with the natural definition of the small gas parameter $\eta_B = -1/\ln(n_B a_{\text{BB}}^2)$ which identifies the boson-boson interaction strength.

In principle, a Bogoliubov treatment of the boson-boson interaction, which implicitly assumes a large condensate fraction, may appear questionable for strong boson-fermion couplings, for which the condensate fraction is significantly depleted. In this regime, however, stability is expected to be guaranteed by fermionization of the BF mixture into a mixture of composite and unpaired fermions, thus making the contribution of η_B in practice immaterial.

The resulting expression of the normal boson self-energy acquires the final form

$$\Sigma_B(\mathbf{k}, \omega) = \Sigma_{11} + \int \frac{d\mathbf{P}}{(2\pi)^2} \int \frac{d\Omega}{2\pi} T(\mathbf{P}, \Omega) G_F^0(\mathbf{P} - \mathbf{k}, \Omega - \omega) e^{i\Omega 0^+}. \quad (10)$$

The diagrams contributing to the fermionic self-energy are of two types, since they originate from closing the T -matrix $T(\mathbf{P}, \Omega)$ either with a normal boson propagator or with two condensate insertions, as Fig. 2(b) shows. However, since the latter choice gives rise to an improper self-energy contribution, to avoid double counting the T -matrix in the normal phase $\Gamma(\mathbf{P}, \Omega)$ is used instead, thus yielding

$$\Sigma_F(\mathbf{k}, \omega) = n_0 \Gamma(\mathbf{k}, \omega) - \int \frac{d\mathbf{P}}{(2\pi)^2} \int \frac{d\Omega}{2\pi} T(\mathbf{P}, \Omega) G_B^0(\mathbf{P} - \mathbf{k}, \Omega - \omega) e^{i\Omega 0^+}. \quad (11)$$

D. Green's functions, momentum distributions, and densities

Once the bosonic and fermionic self-energies are identified, Dyson's equations for the corresponding Green's functions yield

$$G_F^{-1}(\mathbf{k}, \omega) = G_F^0(\mathbf{k}, \omega)^{-1} - \Sigma_F(\mathbf{k}, \omega), \quad (12)$$

$$G_B^{-1}(\mathbf{k}, \omega) = i\omega - \xi_{\mathbf{k}}^B - \Sigma_B(\mathbf{k}, \omega) + \frac{\Sigma_{12}^2}{i\omega + \xi_{\mathbf{k}}^B + \Sigma_B(-\mathbf{k}, -\omega)}. \quad (13)$$

The momentum distributions for fermions and out-of-condensate bosons are obtained in the standard way

$$n_F(\mathbf{k}) = \int_{-\infty}^{+\infty} \frac{d\omega}{2\pi} G_F(\mathbf{k}, \omega) e^{i\omega 0^+}, \quad (14)$$

$$n_B(\mathbf{k}) = - \int_{-\infty}^{+\infty} \frac{d\omega}{2\pi} G_B(\mathbf{k}, \omega) e^{i\omega 0^+} \quad (15)$$

and so their respective number densities

$$n_F = \int \frac{d\mathbf{k}}{(2\pi)^2} n_F(\mathbf{k}), \quad (16)$$

$$n_B = n'_B + n_0 = \int \frac{d\mathbf{k}}{(2\pi)^2} n_B(\mathbf{k}) + n_0. \quad (17)$$

Finally, due to the presence of a bosonic component at zero temperature, the Hugenholtz-Pines condition ([96]) for the corresponding chemical potential is imposed as

$$\mu_B = \Sigma_B(\mathbf{k} = \mathbf{0}, \omega = 0) - \Sigma_{12}. \quad (18)$$

The three equations (16-18) are at the core of our study. They constitute a system of non-linear integral equations whereby the condensate density and the bosonic and fermionic chemical potentials are solved for, once the values of the densities n_B, n_F and scattering lengths a_{BF} and a_{BB} are given.

III. ASYMPTOTIC LIMIT OF STRONG BOSON-FERMION COUPLING

In this section we will examine the regime of strong boson-fermion coupling $\varepsilon_0/E_F \equiv 2e^{2g} \gg 1$ where a simplified and more transparent approach can be adopted. The system of Eqs. (16-18) is replaced with an equivalent but much simpler one, for which a semi-analytical solution can be found. This allows us to disclose the microscopic physics underlying the different concentration regimes ($0 \leq x \leq 1$) in the strong coupling regime ($g > 2$), and, at the same time, to perform stringent checks on crucial physical quantities otherwise obtained through a full numerical implementation. The direct boson-boson repulsion is neglected in the present regime, since it is expected to produce negligible effects.

A. Boson-Fermion propagator $T(\mathbf{P}, \Omega)$

We first delve into the nature of the molecular states through an analysis of the pair propagator $T(\mathbf{P}, \Omega)$. In the limit $\varepsilon_0/E_F \gg 1$, the two contributions in Eq. (5) to the T -matrix $\Gamma(\mathbf{P}, \Omega)$ acquire a simplified form. The first one (see Appendix A, Eq. (A3)) reduces to the polar form

$$T_2(\mathbf{P}, \Omega) \approx \frac{2\pi\varepsilon_0}{m_r} \frac{1}{i\Omega - \frac{P^2}{2M} + \mu_{CF}}, \quad (19)$$

with $\mu_{CF} \equiv \mu_F + \mu_B + \varepsilon_0$ the chemical potential of the composite fermions, whereas the second contribution (see Appendix A, Eq. (A4)) stems from the atomic fermions and reduces to

$$I_F(\mathbf{P}, \Omega) \approx \int \frac{d\mathbf{p}}{(2\pi)^2} \frac{\Theta(-\xi_{\mathbf{P}-\mathbf{p}}^F)}{\varepsilon_0} = \frac{n_{\mu_F}^0}{\varepsilon_0}, \quad (20)$$

where $n_{\mu_F}^0$ is the number density of a non-interacting Fermi gas with chemical potential μ_F . When Eqs. (19) and (20) are inserted into Eq. (5), the latter acquires the strong coupling form

$$\Gamma_{SC}(\mathbf{P}, \Omega) \approx \frac{2\pi\varepsilon_0}{m_r} \frac{1}{i\Omega - \frac{P^2}{2M} + \mu_{CF} - \frac{2\pi}{m_r} n_{\mu_F}^0} \quad (21)$$

which suggests the presence of an effective self-energy term $\Sigma_{CF} = 2\pi n_{\mu_F}^0/m_r$. The latter represents an effective repulsion field generated by the medium of atomic fermions ($\mu_F > 0$) onto the existing molecules, and is an effective way to take into account the kinetic energy cost of populating the molecular Fermi sphere in addition to the atomic one. Through the constant form factor $2\pi\varepsilon_0/m_r$, stemming from the composite nature of the molecules, the above T -matrix $\Gamma_{SC}(\mathbf{P}, \Omega)$ ends up being proportional to a bare fermionic Green's function $G_{CF}^0(\mathbf{P}, \Omega)^{-1} = i\Omega - P^2/2M + \mu_{CF} - \Sigma_{CF}$ dressed by the mean-field of the atomic medium.

In 2D the three-body T -matrix in vacuum, when treated within the Born approximation, reduces to a constant value $2\pi/m_r$, implying that Σ_{CF} is a Hartree contribution of the interaction between the molecular and atomic species (see Appendix B). The atom-molecule scattering length is actually expected to vanish in the strong-coupling limit of the BF interaction [97]. The coupling-independent atom-molecule scattering length obtained by the present approach thus overestimates the atom-molecule repulsion.

Being a mere mean-field shift, Σ_{CF} can be absorbed into a redefinition of the chemical potential in Eq. (19), $\mu_{CF} \rightarrow \tilde{\mu}_{CF} = \mu_{CF} - \Sigma_{CF}$, thus leading to

$$\Gamma_{SC}(\mathbf{P}, \Omega) \approx \frac{2\pi\varepsilon_0}{m_r} \frac{1}{i\Omega - \frac{P^2}{2M} + \tilde{\mu}_{CF}}. \quad (22)$$

Atomic fermions can also correlate with bosons belonging to the condensate during a pair-breaking event (see Fig. 1(b)); this process is taken into account in the dressed propagator $T(\mathbf{P}, \Omega)$ as a self-energy insertion in the related Dyson's (or

Bethe-Salpeter) equation (7) which in the strong coupling limit acquires the form

$$T_{SC}^{-1}(\mathbf{P}, \Omega) = \Gamma_{SC}^{-1}(\mathbf{P}, \Omega) - n_0 G_F^0(\mathbf{P}, \Omega) \\ = \frac{m_r}{2\pi\varepsilon_0} \left(i\Omega - \frac{P^2}{2M} + \tilde{\mu}_{CF} - \frac{\frac{2\pi\varepsilon_0 n_0}{m_r}}{i\Omega - \frac{P^2}{2m_F} + \mu_F} \right) \quad (23)$$

$$\equiv \frac{m_r}{2\pi\varepsilon_0} G_{CF}^{-1}(\mathbf{P}, \Omega) \quad (24)$$

with $G_{CF}(\mathbf{P}, \Omega)$ indicating the dressed composite fermion propagator.

The quantity $2\pi\varepsilon_0 n_0/m_r \equiv \Delta_0^2$ naturally arises as an energy scale associated with exchange of bosons with the condensate and reveals its meaning through an analysis of the pole structure of $T_{SC}(\mathbf{P}, \Omega)$, by which one finds that the resulting dispersion relations

$$E_{\mathbf{P}}^{\pm} = \frac{\tilde{\xi}_{\mathbf{P}}^{CF} + \xi_{\mathbf{P}}^F \pm \sqrt{(\tilde{\xi}_{\mathbf{P}}^{CF} - \xi_{\mathbf{P}}^F)^2 + 4\Delta_0^2}}{2} \quad (25)$$

denote hybridization of a bare molecule (with dispersion $(\tilde{\xi}_{\mathbf{P}}^{CF} = P^2/2M - \tilde{\mu}_{CF})$ with an unpaired atom (with dispersion $\xi_{\mathbf{P}}^F = P^2/2m_F - \mu_F$) and a boson in the condensate (with vanishing kinetic energy). This effect was originally pointed out in [62] for a two-channel model, and signals the inception of strongly renormalized molecular states. These states will be discussed at length in Sec. III D after the thermodynamic parameters will have been consistently determined.

The pair propagator $G_{CF}(\mathbf{P}, \Omega)$ acquires a simple form when expressed in terms of the quasi-particle energies $E_{\mathbf{P}}^{\pm}$ and corresponding weights $u_{\mathbf{P}}^2$ and $v_{\mathbf{P}}^2$,

$$G_{CF}(\mathbf{P}, \Omega) = \frac{u_{\mathbf{P}}^2}{i\Omega - E_{\mathbf{P}}^+} + \frac{v_{\mathbf{P}}^2}{i\Omega - E_{\mathbf{P}}^-} \quad (26)$$

with

$$u_{\mathbf{P}}^2 = \frac{1}{2} \left(1 + \frac{\tilde{\xi}_{\mathbf{P}}^{CF} - \xi_{\mathbf{P}}^F}{\sqrt{(\tilde{\xi}_{\mathbf{P}}^{CF} - \xi_{\mathbf{P}}^F)^2 + 4\Delta_0^2}} \right) \quad \text{and} \quad v_{\mathbf{P}}^2 = 1 - u_{\mathbf{P}}^2. \quad (27)$$

As a consequence, the number of composite fermions n_{CF} is swiftly obtained for given coupling and population imbalance as

$$n_{CF} = \int \frac{d\mathbf{P}}{(2\pi)^2} \int \frac{d\Omega}{2\pi} G_{CF}(\mathbf{P}, \Omega) e^{i\Omega 0^+} \\ = \int \frac{d\mathbf{P}}{(2\pi)^2} [u_{\mathbf{P}}^2 \Theta(-E_{\mathbf{P}}^+) + v_{\mathbf{P}}^2 \Theta(-E_{\mathbf{P}}^-)]. \quad (28)$$

The above integral has a fully analytical form, which is given in Eq. (D1) of appendix D. In practice, however, only the term containing $v_{\mathbf{P}}^2$ contributes, since $E_{\mathbf{P}}^+$ is always positive in the coupling range of interest here.

In conclusion, we have found that molecular BF states are: i) renormalized by the presence of the remaining unpaired

fermions via the mean-field self-energy Σ_{CF} , and ii) hybridized with atomic states owing to pair-breaking fluctuations that foster a non-vanishing condensate. For small bosonic concentrations, the latter feature can also be viewed as feedback of polaronic correlations on the two-body correlator $T(\mathbf{P}, \Omega)$.

B. Fermionic self-energy and momentum distribution

We now pass to examine the fermionic self-energy Eq. (11) in the strong coupling limit, that is with $T(\mathbf{P}, \Omega)$ replaced by $T_{\text{SC}}(\mathbf{P}, \Omega)$.

The frequency integration in Eq. (11) is computed via a contour integration on the left-hand side of the complex plane, owing to the presence of the causality factor 0^+ . Therefore, the pole originating from $G_{\text{B}}^0(\mathbf{P} - \mathbf{k}, \Omega - \omega)$ does not contribute and one is left with the following expression

$$\begin{aligned} \Sigma_{\text{F}}(\mathbf{k}, \omega) &= \frac{\Delta_0^2}{i\omega - \tilde{\xi}_{\mathbf{k}}^{\text{CF}}} + \left(\frac{2\pi\varepsilon_0}{m_r} \right) \int \frac{d\mathbf{P}}{(2\pi)^2} \\ &\times \left[\frac{u_{\mathbf{P}}^2 \Theta(-E_{\mathbf{P}}^+)}{i\omega + \xi_{\mathbf{P}-\mathbf{k}}^{\text{B}} - E_{\mathbf{P}}^+} + \frac{v_{\mathbf{P}}^2 \Theta(-E_{\mathbf{P}}^-)}{i\omega + \xi_{\mathbf{P}-\mathbf{k}}^{\text{B}} - E_{\mathbf{P}}^-} \right]. \end{aligned} \quad (29)$$

Taking advantage of the fact that $\mu_{\text{B}} \simeq -\varepsilon_0$ is the dominant energy scale in the denominators appearing in the integrand on the r.h.s. of Eq. (29), one is allowed to take $\mathbf{P} = 0$ therein thus obtaining

$$\Sigma_{\text{F}}(\mathbf{k}, \omega) = \frac{\Delta_0^2}{i\omega - \tilde{\xi}_{\mathbf{k}}^{\text{CF}}} + \frac{2\pi\varepsilon_0 n_{\text{CF}}}{i\omega + \xi_{\mathbf{k}}^{\text{B}}}, \quad (30)$$

where we have neglected $E_{\mathbf{P}=0}^{\pm}$ altogether with respect to μ_{B} and where n_{CF} is given by Eq. (28).

The large energy scale ε_0 appearing in the second term on the r.h.s of Eq. (30) is compensated by μ_{B} in the denominator, thus making the two terms in Eq. (30) of the same order. By conveniently introducing the energy scale

$$\Delta_{\text{CF}}^2 = \frac{2\pi\varepsilon_0 n_{\text{CF}}}{m_r}, \quad (31)$$

the fermionic Green's function reads

$$G_{\text{F}}^{-1}(\mathbf{k}, \omega) = i\omega - \xi_{\mathbf{k}}^{\text{F}} - \frac{\Delta_0^2}{i\omega - \tilde{\xi}_{\mathbf{k}}^{\text{CF}}} - \frac{\Delta_{\text{CF}}^2}{i\omega + \xi_{\mathbf{k}}^{\text{B}}}, \quad (32)$$

which has three poles in the complex plane. One pole is essentially given by $z = -\xi_{\mathbf{k}}^{\text{B}}$ while the other two are roughly given by $z = \tilde{\xi}_{\mathbf{k}}^{\text{CF}}$ and $z = \xi_{\mathbf{k}}^{\text{F}}$. An analogous form was obtained in [98, 99] even though in the normal phase and in 3D.

Before passing to the exact evaluation of Eq. (32) in closed form, it is instructive for its physical interpretation to analyze the limit of small Δ_0/E_{F} , which is expected to occur either when $x \rightarrow 1$ (depletion of the condensate density due to increase of molecule number) or $x \rightarrow 0$ (reduction of the condensate density due to decrease of boson number). This analysis will provide us with a clear decomposition of $n_{\text{F}}(\mathbf{k})$

into its atomic and molecular contributions. By expanding $G_{\text{F}}(\mathbf{k}, \omega)$ to first order in Δ_0/E_{F} , one obtains

$$\begin{aligned} G_{\text{F}}(\mathbf{k}, \omega) &\simeq \frac{1}{i\omega - \xi_{\mathbf{k}}^{\text{F}} - \frac{\Delta_{\text{CF}}^2}{i\omega + \xi_{\mathbf{k}}^{\text{B}}}} + \\ &+ \frac{\Delta_0^2}{(i\omega - \tilde{\xi}_{\mathbf{k}}^{\text{CF}}) \left(i\omega - \xi_{\mathbf{k}}^{\text{F}} - \frac{2\pi n_{\text{CF}}}{m_r} \right)^2}, \end{aligned} \quad (33)$$

where we have further approximated

$$\frac{\Delta_{\text{CF}}^2}{i\omega + \xi_{\mathbf{k}}^{\text{B}} + \mu_{\text{CF}}} \simeq -\frac{\Delta_{\text{CF}}^2}{\mu_{\text{B}}} = \frac{2\pi n_{\text{CF}}}{m_r} \equiv \Sigma_{\text{F}}^0 \quad (34)$$

in the denominator of the second term. The quantity $2\pi n_{\text{CF}}/m_r \equiv \Sigma_{\text{F}}^0$ is analogous to Σ_{CF} of Sec. III A in that it represents the repulsion induced by the mean-field of the molecules onto the unpaired fermions and can be interpreted as a Hartree mean-field shift ($\tilde{\mu}_{\text{F}} \equiv \mu_{\text{F}} - \Sigma_{\text{F}}^0$).

Let us first consider the first term in Eq. (33). It can be recast in the more familiar (BCS-like) form

$$\frac{\tilde{u}_k^2}{i\omega - \bar{E}_k^+} + \frac{\tilde{v}_k^2}{i\omega - \bar{E}_k^-} \quad (35)$$

with

$$\bar{E}_k^{\pm} = \frac{1}{2} \left(\xi_{\mathbf{k}}^{\text{F}} - \xi_{\mathbf{k}}^{\text{B}} \pm \sqrt{(\xi_{\mathbf{k}}^{\text{F}} + \xi_{\mathbf{k}}^{\text{B}})^2 + 4\Delta_{\text{CF}}^2} \right) \quad (36)$$

and

$$\tilde{u}_k^2 = \frac{1}{2} \left(1 + \frac{\xi_{\mathbf{k}}^{\text{F}} + \xi_{\mathbf{k}}^{\text{B}}}{\sqrt{(\xi_{\mathbf{k}}^{\text{F}} + \xi_{\mathbf{k}}^{\text{B}})^2 + 4\Delta_{\text{CF}}^2}} \right) \quad (37)$$

$$\tilde{v}_k^2 = 1 - \tilde{u}_k^2. \quad (38)$$

We notice that in the asymptotic limit $\varepsilon_0 \gg E_{\text{F}}$, recalling that $\xi_{\mathbf{k}}^{\text{F}} + \xi_{\mathbf{k}}^{\text{B}} \approx \mathbf{k}^2/2m_r + \varepsilon_0$, we can expand the above quantities

$$\bar{E}_k^+ \simeq \tilde{\xi}_{\mathbf{k}}^{\text{CF}}, \quad \bar{E}_k^- \simeq -\xi_{\mathbf{k}}^{\text{B}}, \quad (39)$$

$$\tilde{u}_k^2 \simeq 1 - \frac{\Delta_{\text{CF}}^2}{\left(\frac{\mathbf{k}^2}{2m_r} + \varepsilon_0 \right)^2}, \quad \tilde{v}_k^2 \simeq \frac{\Delta_{\text{CF}}^2}{\left(\frac{\mathbf{k}^2}{2m_r} + \varepsilon_0 \right)^2}. \quad (40)$$

having defined $\tilde{\xi}_{\mathbf{k}}^{\text{CF}} \equiv \xi_{\mathbf{k}}^{\text{F}} + \Sigma_{\text{F}}^0$. Closing the integration contour on the left-hand side of the plane as prescribed by Eq. (14), from the first term in Eq. (33) one obtains the contribution

$$n_{\text{F}}^{(1)}(\mathbf{k}) = \left(1 - \frac{2\pi\varepsilon_0 n_{\text{CF}}}{\left(\frac{\mathbf{k}^2}{2m_r} + \varepsilon_0 \right)^2} \right) \Theta \left(-\tilde{\xi}_{\mathbf{k}}^{\text{CF}} \right) + \frac{2\pi\varepsilon_0 n_{\text{CF}}}{\left(\frac{\mathbf{k}^2}{2m_r} + \varepsilon_0 \right)^2} \quad (41)$$

where one immediately recognizes the squared amplitude of the two-body wave-function in vacuum

$$\phi(\mathbf{k}) = \sqrt{\frac{2\pi\varepsilon_0}{m_r}} \frac{1}{\frac{\mathbf{k}^2}{2m_r} + \varepsilon_0}, \quad (42)$$

multiplied by the number of composite fermions n_{CF} . The second term in Eq. (41) is clearly associated with the composite fermion contribution to $n_{\text{F}}(\mathbf{k})$ whereas the first is due to dressed unpaired fermions as evidenced by the presence of a Fermi step function with argument $-\tilde{\xi}_{\mathbf{k}}^{\text{F}}$ and a quasi-particle weight in front of it.

We now deal with the second term in Eq. (33). It has a pole in $z = \tilde{\xi}_{\mathbf{k}}^{\text{CF}}$ which contributes

$$n_{\text{F}}^{(2)}(\mathbf{k}) = \frac{\Delta_0^2}{(\tilde{\xi}_{\mathbf{k}}^{\text{CF}} - \tilde{\xi}_{\mathbf{k}})^2} \Theta(-\tilde{\xi}_{\mathbf{k}}^{\text{CF}}) \Theta(\tilde{\xi}_{\mathbf{k}}^{\text{F}}), \quad (43)$$

and a double pole in $z = \tilde{\xi}_{\mathbf{k}}^{\text{F}}$ which contributes

$$n_{\text{F}}^{(3)}(\mathbf{k}) = -\frac{\Delta_0^2}{(\tilde{\xi}_{\mathbf{k}}^{\text{CF}} - \tilde{\xi}_{\mathbf{k}}^{\text{F}})^2} \Theta(\tilde{\xi}_{\mathbf{k}}^{\text{CF}}) \Theta(-\tilde{\xi}_{\mathbf{k}}^{\text{F}}). \quad (44)$$

These two terms stem from the second diagram in Fig. 2(b) which favors both pairing with the condensate and atom-

molecule hybridization via the condensate. On physical grounds, for $n_{\text{B}} \ll n_{\text{F}}$ one expects to find weakly interacting atomic fermions, whereas in the opposite limit of $n_{\text{B}} \approx n_{\text{F}}$ one should find the specular situation of weakly interacting molecules. In these two opposite limits one has indeed $\tilde{\mu}_{\text{F}} > 0$, $\tilde{\mu}_{\text{CF}} < 0$ for $x \rightarrow 0$ and $\tilde{\mu}_{\text{CF}} > 0$, $\mu_{\text{F}} < 0$ for $x \rightarrow 1$. Therefore, expression (43) is non-zero for $x \rightarrow 1$, with $\Theta(\tilde{\xi}_{\mathbf{k}}^{\text{F}}) = 1$, whereas expression (44) is non-zero for $x \rightarrow 0$, with $\Theta(\tilde{\xi}_{\mathbf{k}}^{\text{CF}}) = 1$, and is to be summed to the same type of contribution in expression (41).

To sum up, the full fermionic momentum distribution $n_{\text{F}}(\mathbf{k})$ is split as the sum of a contribution $n_{\text{CF}}|\phi(\mathbf{k})|^2$ from fermions bound into molecules, and an unpaired fermion contribution $n_{\text{UF}}(\mathbf{k})$ as follows:

$$n_{\text{F}}(\mathbf{k}) = n_{\text{CF}}|\phi(\mathbf{k})|^2 + n_{\text{UF}}(\mathbf{k}), \quad (45)$$

where

$$n_{\text{UF}}(\mathbf{k}) = \begin{cases} \left[1 - n_{\text{CF}}|\phi(\mathbf{k})|^2 - \frac{\Delta_0^2}{(\tilde{\xi}_{\mathbf{k}}^{\text{CF}} - \tilde{\xi}_{\mathbf{k}}^{\text{F}})^2} \right] \Theta(-\tilde{\xi}_{\mathbf{k}}^{\text{F}}), & x \rightarrow 0 \\ \frac{\Delta_0^2}{(\tilde{\xi}_{\mathbf{k}}^{\text{CF}} - \tilde{\xi}_{\mathbf{k}}^{\text{F}})^2} \Theta(-\tilde{\xi}_{\mathbf{k}}^{\text{CF}}), & x \rightarrow 1. \end{cases} \quad (46a)$$

$$\left(\frac{\Delta_0^2}{(\tilde{\xi}_{\mathbf{k}}^{\text{CF}} - \tilde{\xi}_{\mathbf{k}}^{\text{F}})^2} \Theta(-\tilde{\xi}_{\mathbf{k}}^{\text{CF}}), \quad x \rightarrow 1. \right. \quad (46b)$$

Expressions (46a) and (46b) describe unpaired fermions in two different regimes. In Eq. (46a) atoms are the majority species and most of the fermions are unpaired because of the small number of bosons to pair with. When one inserts the contribution (46a) in Eq. (45) one recovers a nearly filled Fermi sphere, with a small depletion, described by the last term in Eq. (46a). In Eq. (46b) molecules are instead the majority species; the few unpaired fermions are strongly renormalized by interaction with molecules (since $\Delta_0/E_{\text{F}} \ll 1$ and the denominator in Eq. (46b) never vanishes) and partially occupy single-particle states within a Fermi sphere determined by $\Theta(-\tilde{\xi}_{\mathbf{k}}^{\text{CF}})$.

Finally, we consider evaluating the frequency integration of the Green's function (32) to obtain $n_{\text{F}}(\mathbf{k})$ in a closed form without expanding in Δ_0/E_{F} . This can be done analytically on the complex plane by first solving the cubic equation for the three poles z_i , $i = 1, 2, 3$

$$z_i - \xi_{\mathbf{k}}^{\text{F}} - \frac{\Delta_0^2}{z_i - \tilde{\xi}_{\mathbf{k}}^{\text{CF}}} - \frac{\Delta_{\text{CF}}^2}{z_i + \xi_{\mathbf{k}}^{\text{B}}} = 0, \quad (47)$$

and then applying the residue theorem on a contour running along the imaginary axis and closed on the left-hand half of the plane, yielding

$$n_{\text{F}}(\mathbf{k}) = \sum_{i=1}^3 \lim_{z \rightarrow z_i} \frac{z - z_i}{z - \xi_{\mathbf{k}}^{\text{F}} - \frac{\Delta_0^2}{z - \tilde{\xi}_{\mathbf{k}}^{\text{CF}}} - \frac{\Delta_{\text{CF}}^2}{z + \xi_{\mathbf{k}}^{\text{B}}}} \Theta(-z_i). \quad (48)$$

The total number density n_{F} is then evaluated numerically via Eq. (16).

C. Hugenholtz-Pines condition for condensed bosons

In the absence of boson-boson repulsion ($\Sigma_{11} = \Sigma_{12} = 0$) and in the strong coupling limit of interest here, the bosonic self-energy (10) acquires the form

$$\Sigma_{\text{B}}(\mathbf{k}, \omega) = \left(\frac{2\pi\varepsilon_0}{m_r} \right) \int \frac{d\mathbf{P}}{(2\pi)^2} \left[u_{\mathbf{P}}^2 \frac{\Theta(-E_{\mathbf{P}}^+) - \Theta(-\xi_{\mathbf{P}-\mathbf{k}}^{\text{F}})}{E_{\mathbf{P}}^+ - \xi_{\mathbf{P}-\mathbf{k}}^{\text{F}} - i\omega} + v_{\mathbf{P}}^2 \frac{\Theta(-E_{\mathbf{P}}^-) - \Theta(-\xi_{\mathbf{P}-\mathbf{k}}^{\text{F}})}{E_{\mathbf{P}}^- - \xi_{\mathbf{P}-\mathbf{k}}^{\text{F}} - i\omega} \right], \quad (49)$$

after a contour integration on the left-hand side of the complex frequency plane.

This expression is not analytically tractable except when it is evaluated at zero momentum and frequency in the Hugenholtz-Pines condition (18), as shown in Appendix D.

D. Complete system of semi-analytical equations in closed form and their solutions

Collecting the analytic results obtained so far, it turns out that the system of Eqs. (16-18) becomes analytically tractable in the strong coupling limit. Equations (16 and 18) are given in closed form in Eq. (47) and in Eq. (D4) in Appendix D respectively, while Eq. (17) does not have an analytic form. Nevertheless, for large g all bosons out of the condensate are expected to bind to fermions (as $n_B \leq n_F$) hence allowing one to substitute Eq. (17) for bosons with Eq. (28) for composite fermions since $n_B - n_0 \approx n_{CF}$. This replacement is not just a mathematical rearrangement but reflects the physical fact that the system is now effectively a Fermi-Fermi mixture of molecules and unpaired fermions. As a consequence, one obtains the following set of equations for the unknowns μ_F , μ_B and n_0 (and implicitly $\mu_{CF} \equiv \mu_F + \mu_B + \varepsilon_0$):

- Fermion number equation

$$n_F = \int \frac{d\mathbf{k}}{(2\pi)^2} n_F(\mathbf{k}), \quad (50)$$

with $n_F(\mathbf{k})$ given by Eq. (48);

- Composite-fermion number Eq. (28)

$$n_B - n_0 = \int \frac{d^2P}{(2\pi)^2} \left[u_{\mathbf{P}}^2 \Theta(-E_+) + v_{\mathbf{P}}^2 \Theta(-E_-) \right], \quad (51)$$

whose analytical form is given in Eq. D1;

- Hugenholtz-Pines condition (18)

$$\mu_B = \Sigma_B(\mathbf{k} = \mathbf{0}, \omega = 0) = \left(\frac{2\pi\varepsilon_0}{m_r} \right) \int \frac{d\mathbf{P}}{(2\pi)^2} \times \left[\frac{u_{\mathbf{P}}^2}{E_{\mathbf{P}}^+ - \xi_{\mathbf{P}}^F} \Theta(-E_{\mathbf{P}}^+) + \frac{v_{\mathbf{P}}^2}{E_{\mathbf{P}}^- - \xi_{\mathbf{P}}^F} \Theta(-E_{\mathbf{P}}^-) \right], \quad (52)$$

whose analytic expression is given in Eq. D4.

These equations can be solved with a standard root finder, and no particular care has to be taken when performing the related momentum integrations. We now discuss their solutions in the form of the chemical potentials μ_F and μ_B , the hybridization energy Δ_0 and the Fermi momentum distribution profile $n_F(\mathbf{k})$.

In Fig. 3(a) the fermion chemical potential μ_F and the sub-leading correction to the boson chemical potential $\mu_B + \varepsilon_0$ are shown along with the (shifted) composite fermion chemical potential $\tilde{\mu}_{CF} = \mu_{CF} - \Sigma_{CF}$. Trivially, the bosonic chemical potential μ_B follows the dominant energy scale of the binding energy $-\varepsilon_0$, implying that as soon as a boson is added to the system it binds to a fermion ($n_B \leq n_F$). Depending on the sign of the chemical potentials, we distinguish two clearly different yet specular regimes separated by a crossover region roughly given by the range $0.7 \lesssim x \lesssim 0.9$ (shaded region). In line with what obtained in Sec. III B, we confirm that at the left of this region ($n_B \ll n_F$), the system is made

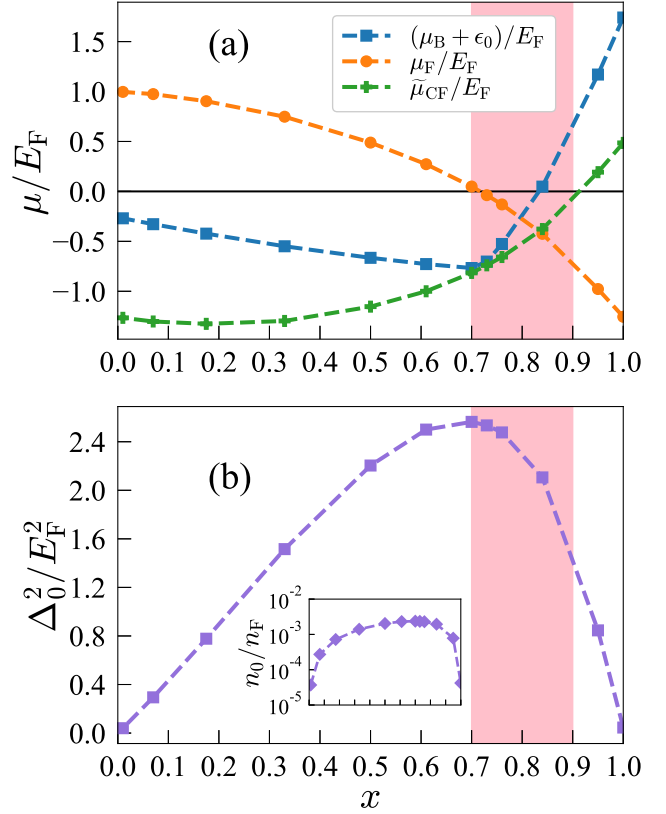


Figure 3. (a): Chemical potentials μ_F , $\mu_B + \varepsilon_0$ and $\tilde{\mu}_{CF} = \mu_{CF} - \Sigma_{CF}$ as functions of concentration x , for strong BF attraction $g = 2.8$ and boson-boson repulsion $\eta_B = 0$. (b): Square of the hybridization energy Δ_0 (in units of E_F^2) as a function of the boson concentration x , for strong BF attraction $g = 2.8$ and boson-boson repulsion $\eta_B = 0$.

of weakly interacting atomic fermions ($\mu_F > 0$) and strongly renormalized molecules ($\tilde{\mu}_{CF} < 0$) whereas at the right of this region ($n_B \approx n_F$), in a specular manner, degenerate molecules ($\tilde{\mu}_{CF} > 0$) and strongly dressed atomic fermions ($\mu_F < 0$) coexist.

In the crossover region, all chemical potentials are comparable in size and on the verge of changing sign: here atoms and molecules are in a state of maximal hybridization as reflected in Fig. 3(b) where the hybridization energy squared $\Delta_0^2/E_F^2 = 2\varepsilon_0 n_0/E_F n_F$ defined in Sec. III A is reported. The inversion of behavior of Δ_0 as a function of x approximately matches the inversion of sign of the chemical potentials, being peaked exactly when $\mu_F \approx 0$. In the inset of Fig. 3(b) the condensate density n_0 is also displayed to show its exponentially suppressed value, compensated by the exponential increase of the binding energy in the resulting Δ_0 .

Let us now analyze in detail the effect of the hybridization scale Δ_0 through the energy spectrum $E_{\mathbf{P}}^{\pm}$ of the molecular quasi-particles defined by Eq. (25) of Sec. III A. In Fig. 4 the dispersions $E_{\mathbf{P}}^{\pm}$ are compared with those of the bare (molecular and atomic) fermions for coupling $g = 2.8$ and different values of the boson concentration x . At exactly matched densities ($x = 1$) all fermions are essentially paired with all bosons

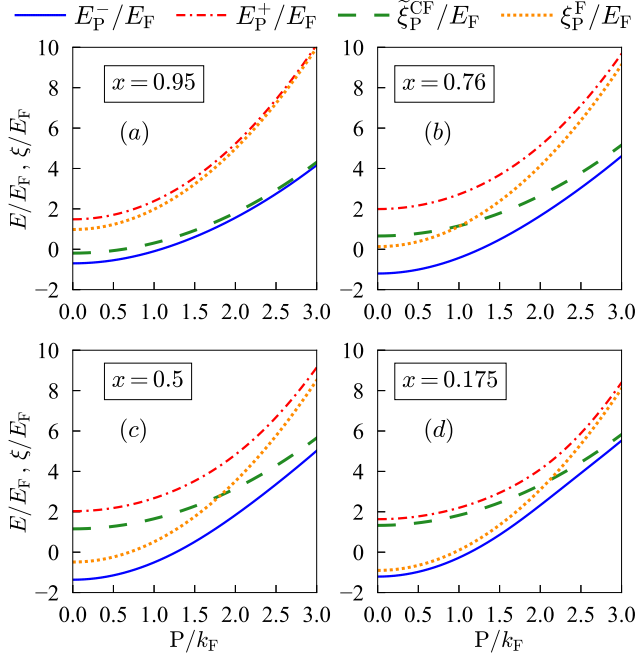


Figure 4. Dispersions $E_{\mathbf{P}}^{\pm}$ of the poles of the strong-coupling limit T -matrix $T_{\text{SC}}(\mathbf{P}, \Omega)$ and bare molecular and atomic Fermi dispersions $\xi_{\mathbf{P}}^{\text{CF}}$ and $\xi_{\mathbf{P}}^{\text{F}}$, respectively. All data are obtained for strong BF attraction $g = 2.8$ and several bosonic concentrations: (a) $x = 0.95$, (b) $x = 0.76$, (c) $x = 0.5$, (d) $x = 0.175$.

($n_0 \approx 0$) and the system is effectively made of a gas of non-interacting molecules, with the bare dispersions coinciding with the dressed one since $\Delta_0 \approx 0$.

As soon as a population imbalance sets in x (see the case $x = 0.95$ in Fig. 4(a)), the hybridization energy scale Δ_0 sharply rises and hybrid quasi-particles form out of the molecular and unpaired Fermi states. This phase approximately corresponds to the extreme right of Fig. 3(a)-(b). As population imbalance further increases, even though n_0 remains exponentially suppressed ($n_0 \propto \Delta_0^2/\varepsilon_0$), the presence of a non-zero Δ_0 stabilizes the system by lowering the energy dispersion $E_{\mathbf{P}}^-$ with respect to the bare one $\xi_{\mathbf{k}}^{\text{CF}}$. This effect is rooted in the kinetic energy cost when filling up the paired and unpaired Fermi spheres: in order to reduce it, the molecular and atomic wave-functions hybridize quantum-mechanically by overlapping with the condensate wave-function (thus gaining in delocalization energy). The bottom panels of Fig. 4 display the typical level crossing (dotted lines) and avoided crossing (dashed lines) of a non-hybridized and hybridized two-level system, respectively. At the crossover concentration $x \approx 0.7$, the hybridization is about maximal and the character of the occupied states (bottom pole dispersion) switches from molecular to mostly atomic as x is reduced (with an effective mass approaching m_{F}). At small concentration ($x = 0.175$) the dispersion of occupied states approaches the limit of the weakly interacting Fermi gas $\xi_{\mathbf{k}}^{\text{F}}$ (dressed impurity limit) with vanishing quasi-particle weight $v_{\mathbf{P}}^2 \approx 0$, in line with the extreme left region of Fig. 3(a)-(b).

In Fig. 5 the quasi-particle weight $v_{\mathbf{P}}^2$ of the occupied states

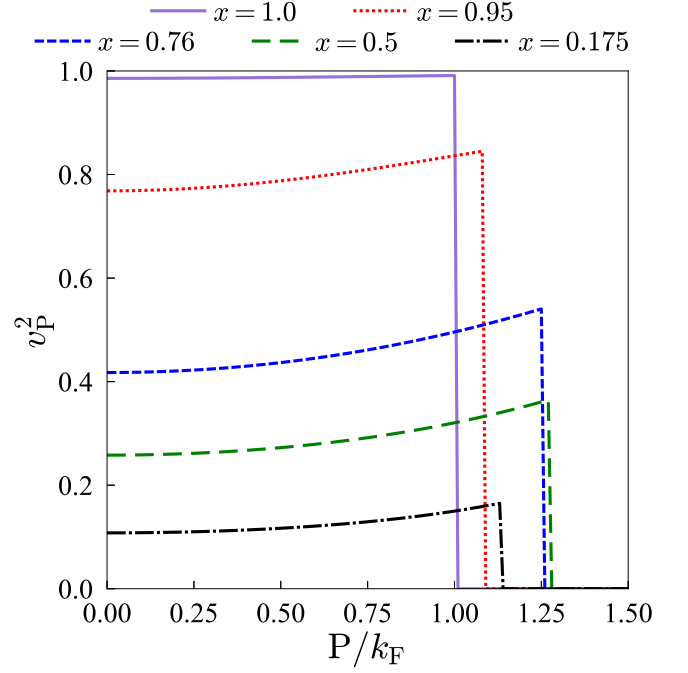


Figure 5. Quasi-particle weight $v_{\mathbf{P}}^2$ of Eq. (27) corresponding to the momentum distribution of the hybridized composite fermions for BF coupling $g = 2.8$ and concentrations matching those in Fig. 4, along with the case $x = 1$.

$\Theta(-E_{\mathbf{P}}^-)$ is displayed for a number of concentrations corresponding to those in Fig. 4 along with the case $x = 1$. In the latter case, the mixture is essentially made of a single component gas of non-interacting point-like fermionic molecules, as illustrated by the Fermi step behavior with occupation number approaching unity. As x decreases, the quasi-particle nature of the occupied states due to the hybridization of the molecular states with atomic ones becomes significant, producing a rather peculiar behavior of the momentum distribution function, as evidenced by its upward bending as the momentum increases, and by the position of the Fermi step, that, in particular for small concentration, is well above the expected position if one would assume the Luttinger theorem to be valid for the composite fermions. This is different with respect to the 3D case, where the Luttinger theorem was found to be respected by the composite fermions in the strong-coupling limit [81]. In that case, however, no hybridization occurred since the condensate vanished above a critical coupling, thus yielding essentially the same picture that we obtain here only at $x = 1$. We further notice that in 2D the breakdown of the Luttinger theorem for the hybridized composite fermions is compensated, as far as the integrated quantity $n_{\text{CF}} = \int \frac{d\mathbf{P}}{(2\pi)^2} v_{\mathbf{P}}^2 \Theta(-E_{\mathbf{P}}^-)$ is concerned, by the strong suppression of the weight $v_{\mathbf{P}}^2$ when the concentration decreases, in such a way that the identification of n_{CF} with $n_{\text{B}} - n_0 \approx n_{\text{B}}$ is always valid in the strong-coupling limit.

Finally, we discuss the profiles of the Fermi momentum distribution (48) for fixed coupling strength and varying concentration. This allows us to confirm the analysis of the molecular and atomic states done above and identify the contributions of

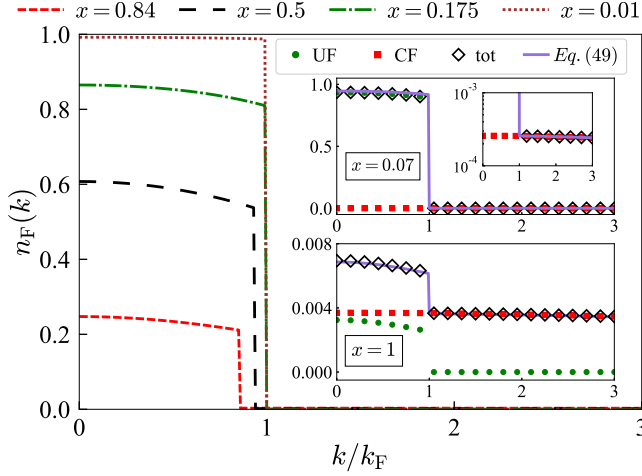


Figure 6. Fermionic momentum distribution as obtained from the strong-coupling limit expression (48) for various bosonic concentrations x at BF coupling $g = 2.8$. In the insets the same expression is broken down into the analytical contributions (45), (46a) and (46b), for small and large x where these formulae apply.

paired and unpaired fermions given by expressions (45), (46a) and (46b) of Sec. III B. In Fig. 6 $n_F(\mathbf{k})$ is displayed for $g = 2.8$ and different values of x . For small x , a weakly renormalized Fermi step is found in line with a majority of weakly dressed unpaired fermions (46a) and a minority of molecules pictured by the small tail of their internal wave-function (45). As x increases, the height of the Fermi step is reduced by the interaction with the bosons, until x approaches 1 whereby the position of the Fermi step is again associated with the majority fermions, now coming from molecules, but with its height given by the quasi-particle weight $\Delta_0^2 / (\tilde{\xi}_k^{\text{CF}} - \tilde{\xi}_k)^2$ of a minority of strongly hybridized unpaired fermions (46b).

The above considerations are quantitatively illustrated in the insets of Fig. 6 for large ($x = 1$) and small ($x = 0.07$) concentrations. Therein, the distribution function (45) is broken down in paired (CF) and unpaired (UF) contributions, and compared with the exact expression (48). In the top inset we find a small contribution from molecules (CF) and a majority of unpaired fermions (UF), whereas in the bottom panel molecules (CF) are the majority species and unpaired fermions are strongly renormalized (UF).

We thus find a consistent picture throughout the diverse thermodynamic quantities in all regimes originally identified in the different regions of Fig. 3.

IV. NUMERICAL RESULTS

In this section, we present the fully numerical results for the boson and fermion momentum distributions and for key thermodynamic quantities like the chemical potentials and condensate fraction with varying coupling strength. We also discuss the results for the Tan's contact parameter [100–102].

A. Methods

We recall the system of equations constituting the bulk of our numerical calculations

$$\mu_B = \Sigma_B(\mathbf{k} = \mathbf{0}, \omega = 0) - \Sigma_{12} \quad (53a)$$

$$n_F = \int \frac{d\mathbf{k}}{(2\pi)^2} n_F(\mathbf{k}) \quad (53b)$$

$$n_B = n_0 + n'_B = n_0 + \int \frac{d\mathbf{k}}{(2\pi)^2} n_B(\mathbf{k}). \quad (53c)$$

For given values of n_F, n_B, a_{BF} and a_{BB} the above system is solved for the unknowns μ_F, μ_B and n_0 , as follows. First a solution is found for μ_B from Eq. (53a) with a standard bisection method assuming a suitable ansatz for μ_F and n_0 . Then we consider the 2×2 system of the remaining Eqs. (53b) and (53c) as functions of μ_F and n_0 and apply a two-dimensional secant (quasi-Newton) method whereby the approximate Jacobian matrix (which corresponds to the approximate Hessian of the total energy) is updated according to a symmetric rank 1 algorithm [103], that is a generalization of the secant method to multidimensional problems.

An intermediate step of the above procedure is the evaluation of the bosonic and fermionic self-energies, which requires, owing to the low dimensionality of the problem at hand, special care when dealing with the slow convergence of the frequency convolutions appearing in Eqs. (10)-(11). In order to speed up the convergence, the integrand of the convolutions is added and subtracted by an auxiliary function with the same asymptotic behavior yet analytically integrable. As a result, the numerical integration is truncated by applying a large frequency cutoff, which we fix at $\Omega_c = \pm 50000 E_F$ after an accurate analysis of the asymptotic behaviors. For $|\Omega| \geq \Omega_c$ integration is done making use of asymptotic expressions whose details are provided in Appendix C. In addition, integration in momentum space is affected by the presence of discontinuities in the integrand due to Fermi steps. Therefore, a careful analysis of the location of these discontinuities is performed in order to identify the appropriate integration intervals, for which a standard Gauss-Legendre quadrature method is adopted [104]. The largest Fermi momentum provides a natural cutoff for the momentum convolutions defining both bosonic and fermionic self-energies.

Concerning the frequency integral yielding the momentum distributions (14) and (15) we take advantage of the large frequency behavior of the self-energies (C5-C6) valid in the range $|\omega| \geq 100 E_F$, whereas for $|\omega| < 100 E_F$ we integrate the full numerical expression (see Appendix C 2). Momentum integration in expressions (16) and (17) is carried out numerically up to a cutoff of $k_c = 4k_F$, after having subtracted and added a non-interacting or a Bogoliubov Green's function respectively (see Appendix C 2), and beyond k_c by making use of the asymptotic expressions (60-61).

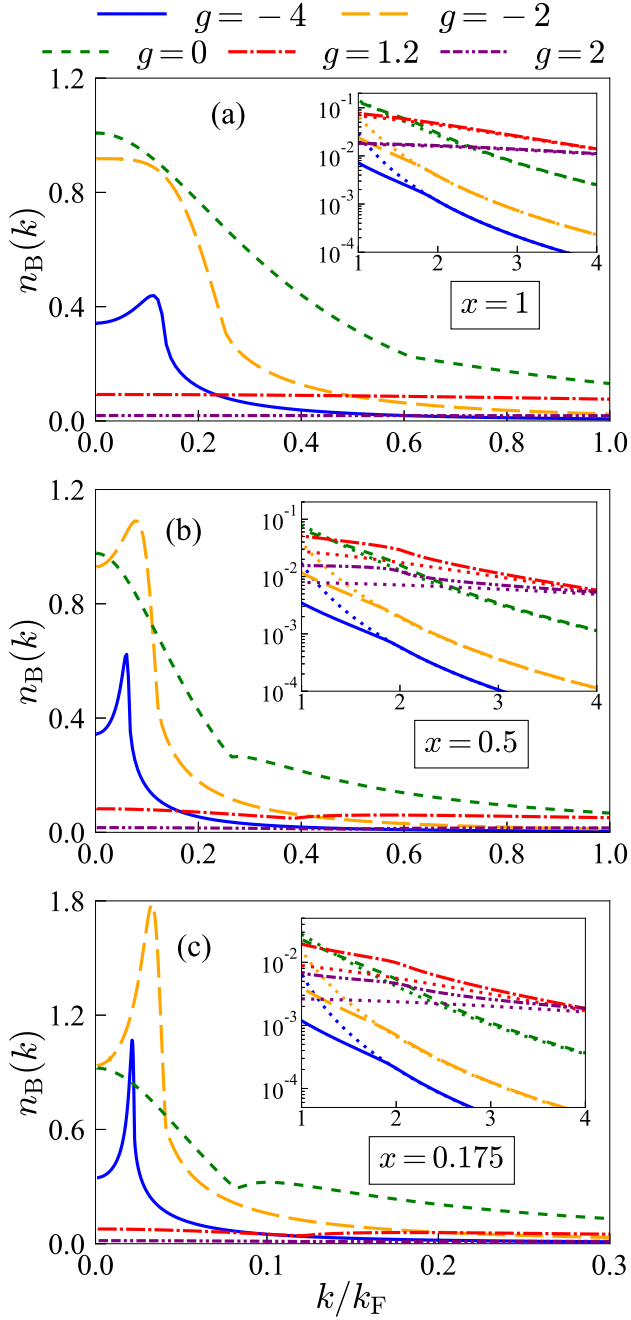


Figure 7. Bosonic momentum distribution $n_B(k)$ as a function of k/k_F , for different values of BF coupling g at boson-boson repulsion $\eta_B = 0$. Different cases of bosonic concentration x are reported: (a) $x = 1$, (b) $x = 0.5$, (c) $x = 0.175$. Insets: comparison at large momenta between numerical results and asymptotic behavior (dotted lines) reported in Eq. (61).

B. Boson and fermion momentum distributions

We now discuss the numerical results for the fermionic and bosonic momentum distributions, Eqs. (14)-(15). Figure 7 shows the bosonic momentum distribution from weak to strong

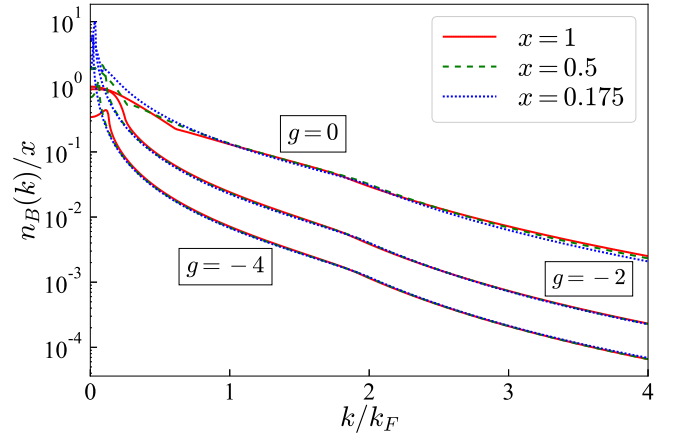


Figure 8. Bosonic momentum distribution $n_B(k)$ divided by the boson concentration x for several values of x and BF coupling g .

BF coupling for different bosonic concentrations x and zero bosonic repulsion, $\eta_B = 0$. A peculiar feature common to all panels is the appearance of a peak for small but non-zero momenta, depending on the concentration and coupling. In particular, for very weak coupling the peak persists for all concentrations (full line in all panels) in contrast to higher couplings where it soon disappears. One is thus led to think that a weak-coupling mean-field effect may be at the origin of the peak, primarily due to the unpaired atoms dressing up the weakly interacting bosons, hence a sort of polaronic effect. However, for a definite identification of this peak, an analysis of the bosonic spectral weight function would be in order (this is postponed to future work).

At large k , the momentum distribution is expected to be dominated by short-range pairing correlations captured by the asymptotic expression (61) (with the anomalous self-energy turned off in this case). The insets in Fig. 7 compare the numerical large- k behavior of $n_B(\mathbf{k})$ with the corresponding asymptotic expression (61) (dotted lines).

In strict analogy to what found in 3D [88], and preparing for the universality of the condensate fraction that will be illustrated in Sec. IV D, it is instructive to inspect the boson momentum distribution divided by the boson concentration x . Figure 8 shows that the momentum distributions $n_B(\mathbf{k})$ corresponding to different values of x collapse on top of each other once divided by the concentration x , except for a region at small \mathbf{k} . This universality, which occurs from weak to intermediate coupling ($g \lesssim 0$), suggests that in this coupling range the bosons can be treated as nearly independent of each other (but interacting with the medium), such that $n_B(\mathbf{k}) \simeq n_B n_{x \rightarrow 0}(\mathbf{k})$, with $n_{x \rightarrow 0}(\mathbf{k}) \equiv \lim_{x \rightarrow 0} n_B(\mathbf{k})/n_B$. We stress that this is not obvious a priori, even in the absence of a direct BB repulsion (as in the case we are considering here), since indirect interactions mediated by the fermions are possible. Indeed, this is what happens at small momenta k , as signalled by the deviation of $n_B(\mathbf{k})$ from such independent particle picture in this momentum range.

An interesting feature is also observed when plotting the limiting value for vanishing momentum ($n_B(\mathbf{k} \rightarrow 0)$) of the

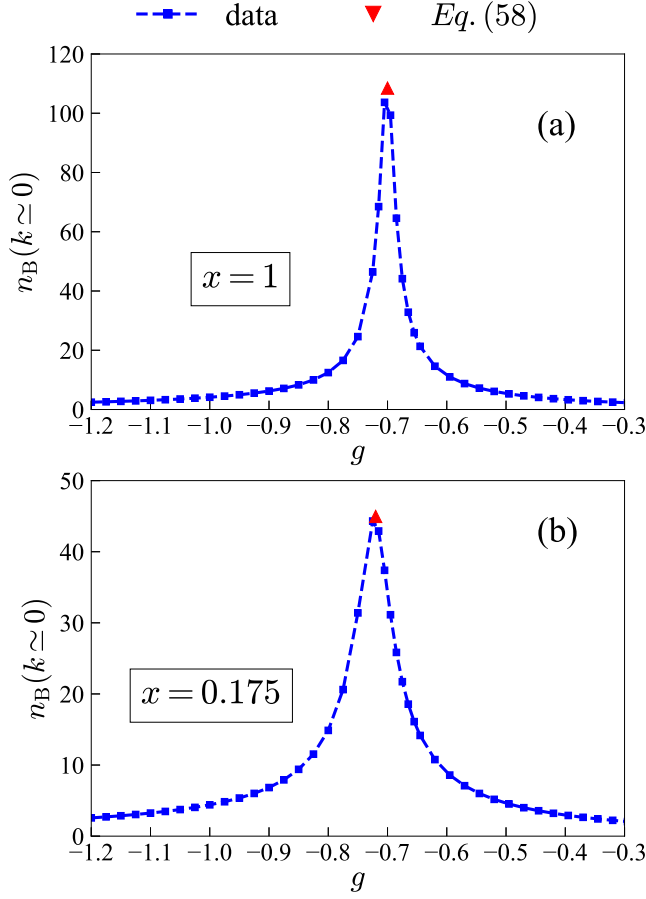


Figure 9. Bosonic momentum distribution $n_B(k)$ evaluated at small momentum $k \approx 0.003k_F$ as a function of BF coupling g , at boson-boson repulsion $\eta_B = 0$, for bosonic concentration (a) $x = 1$ and (b) $x = 0.175$. Triangle: peak value obtained from Eq. (57). Dashed line: guide to the eye.

momentum distribution of non-condensed bosons as a function of coupling, as shown in Fig. 9 for two representative values at large and small boson concentrations. By keeping k/k_F fixed at small value and scanning the BF interaction, a prominent peak appears close to $g \approx -0.7$ which eventually diverges in the limit $k = 0$. We stress that in the present case the BB repulsion is turned off and thus there is no anomalous self-energy term (which would yield $n_B(\mathbf{k} \rightarrow 0) \rightarrow \infty$ for all values of g , as standard from Bogoliubov theory).

It is possible to elucidate the origin of this behavior by assuming a generic expansion for the boson self-energy at small \mathbf{k} and ω

$$\Sigma_B(\mathbf{k}, \omega) = \Sigma_B(0, 0) + a i\omega + b \omega^2 + c k^2, \quad (54)$$

with a, b, c , real. When inserted in Eq. (13) with $\Sigma_{12} = 0$, Eq. (54) yields

$$G_B(\mathbf{k}, \omega) \simeq \frac{1}{(1-a)i\omega - \frac{k^2}{2m_B^*} - b\omega^2} \quad (55)$$

where $1/m_B^* = 1/m_B + c$ and the Hugenholtz-Pines condition has been used. By fitting the coefficients a, b, c with the data for the boson self-energy at small ω and \mathbf{k} , we find that, at $g \approx -0.7$, $a = 1$ and b is positive, resulting in the following expression for the momentum distribution (15)

$$n_B(\mathbf{k}) \simeq \int_{-\omega_{\text{IR}}}^{+\omega_{\text{IR}}} \frac{d\omega}{2\pi} \frac{1}{\frac{k^2}{2m_B^*} + b\omega^2} + 2 \int_{\omega_{\text{IR}}}^{+\infty} \frac{d\omega}{2\pi} \Re[G_B(\mathbf{k}, \omega)], \quad (56)$$

where ω_{IR} is an appropriate infrared cutoff defining the range of validity of the above expansion. For small enough \mathbf{k} the second integral is a subleading contribution and one obtains to leading order

$$n_B(\mathbf{k}) \approx \frac{1}{2} \sqrt{\frac{m_B^*}{m_F}} \frac{1}{bE_F} \frac{k_F}{k}, \quad k \rightarrow 0. \quad (57)$$

One sees in Fig. 9 that this asymptotic expression matches well the peak value of $n_B(k \approx 0)$ as a function of g .

This short exercise reveals that at $g \approx -0.7$ the energy spectrum at small momenta provided by the poles of the Green's function (55) changes from being quasi-particle like ($\omega \propto \pm k^2$ when $a \leq 1$, respectively) to collective (phononic) mode type ($\omega^2 \propto k^2$ when $a = 1$). In contrast to the weakly repulsive Bose gas where the energy spectrum is given by $\omega^2 = c_s^2 k^2$ with c_s the sound velocity, here the latter turns out to be purely imaginary ($\omega^2 = -k^2/(2m_B^* b)$) implying the mechanical instability of the Bose component. This is not unexpected since the indirect interaction among bosons mediated by the fermionic medium is attractive at any coupling [3] thus making the mixture mechanically unstable per se. However, we note that the microscopic mechanism of mechanical collapse is generally due to quasi-particle or incoherent excitations [81], except for $g \approx -0.7$ where instead a phononic collective mode sets in.

For this reason one needs to include a BB repulsion in order to stabilize the system against the aforementioned effects. We thus consider the case where a direct BB repulsion is turned on, causing a divergence at zero k to be present at all g 's, as expected within Bogoliubov theory. Calculations for a relatively strong boson-boson repulsion $\eta_B = 0.1$ are reported in Fig. 10. Clearly, the main differences with respect to the case of zero repulsion occur at small momenta, where the occupation of low momenta states predicted by Bogoliubov theory dominates. Regarding the large momentum regime (not reported in Fig. 10), it is well described by expression (61) discussed below.

Concerning the Fermi momentum distribution we first discuss its comparison with the strong-coupling expression (48) with a two-fold aim: to untangle the different contributions from bare or dressed atoms and molecules based on the lesson learned in Sec. III and, at the same time, to perform a stringent check on our numerical implementation. Fig. 11 displays the numerical results for $n_F(\mathbf{k})$ as symbols and the expression (48) as lines for several values of BF coupling g and (a) $x = 1$, (b)

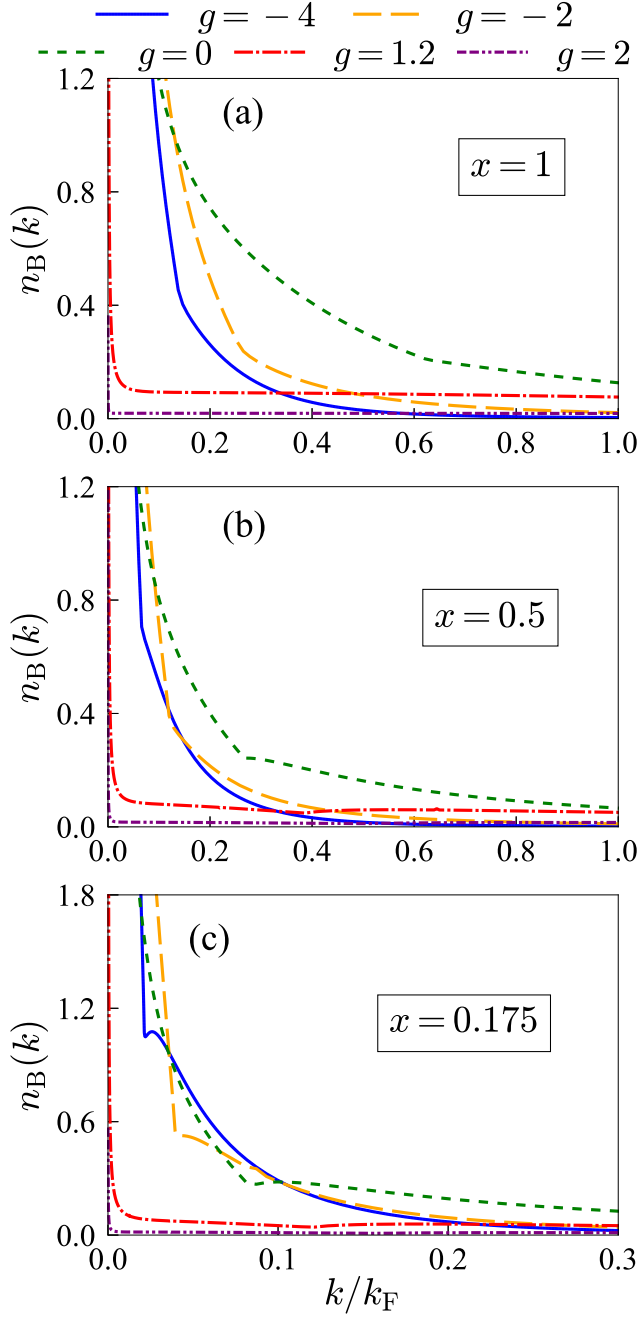


Figure 10. Bosonic momentum distribution $n_B(k)$ as a function of momentum k/k_F , for different values of boson-fermion coupling g at boson-boson repulsion $\eta_B = 0.1$. Different cases of bosonic concentration x are reported: (a) $x = 1$; (b) $x = 0.5$; (c) $x = 0.175$.

$x = 0.5$ (c) $x = 0.175$, using the same thermodynamical parameters for both sets of curves. The agreement is remarkably good for $g \geq 0$, thus demonstrating that the fermionic Green's function is well captured by the BCS-like expression (32) in an extended coupling range and not only for large values of g . We note that the discussion on paired and unpaired fermions of Sec. III applies here, with the tail of $n_F(\mathbf{k})$ representing the molecular wave-function and the Fermi step measuring

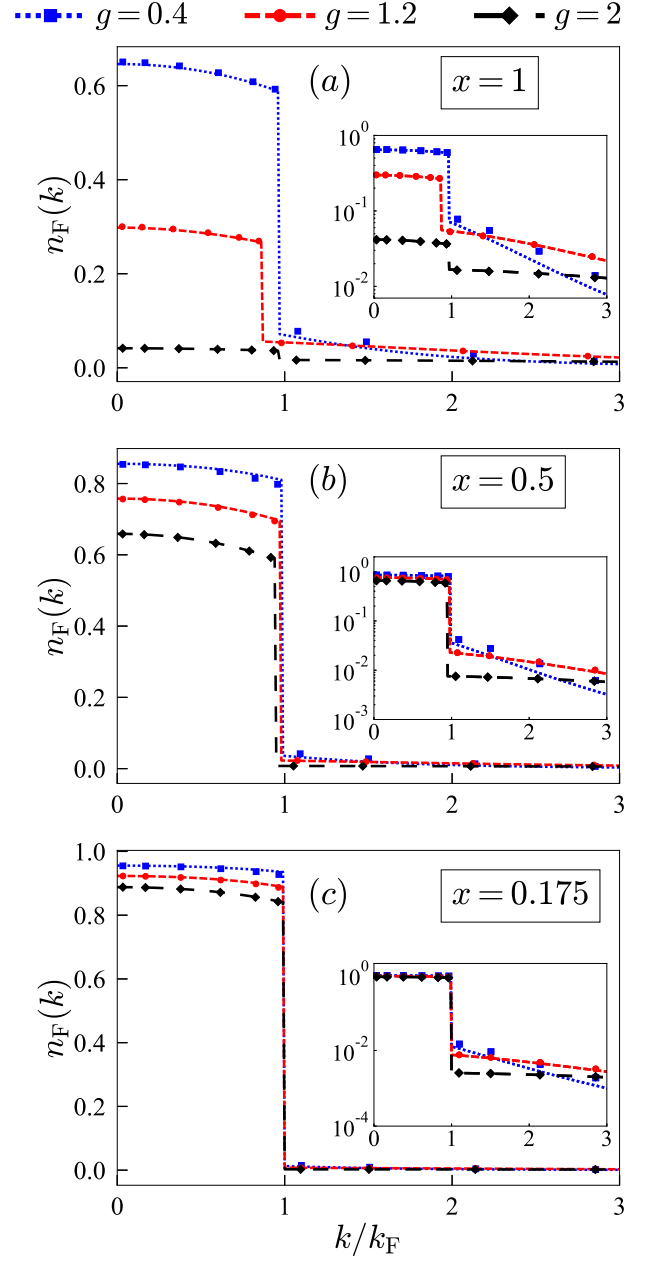


Figure 11. Fermionic momentum distribution for bosonic concentrations (a) $x = 1$, (b) $x = 0.5$ and (c) $x = 0.175$ and different values of boson-fermion coupling at boson-boson repulsion $\eta_B = 0$. Symbols indicate numerical data, while lines are their analytical benchmark. The same thermodynamical parameters are employed in the calculation of both sets of curves. Insets: same quantities in log-scale.

the amount of unpaired yet correlated fermions. We notice that, when g is reduced, discrepancies between the asymptotic curve and numerical data occur first for higher boson concentration, and they occur in the tail of $n_F(\mathbf{k})$. This is related to the onset of the continuum of particle-hole excitations becoming comparable to the molecular binding energy, thus making the BCS-like expression (48) less valid.

For generic coupling strength, the numerical Fermi mo-

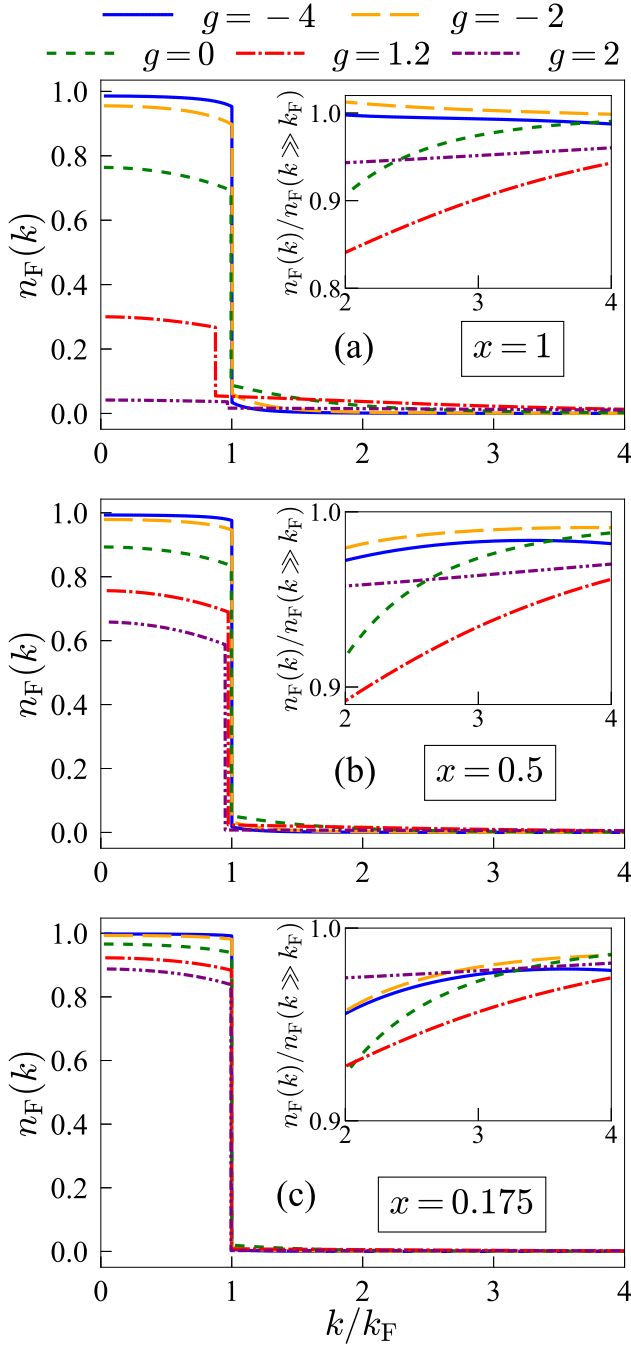


Figure 12. Fermionic momentum distribution $n_F(k)$ as a function of momentum k/k_F , for different values of BF coupling g at boson-boson repulsion $\eta_B = 0$. Different cases of bosonic concentration x are reported: (a) $x = 1$, (b) $x = 0.5$, (c) $x = 0.175$. Insets: ratio of $n_F(k)$ to its asymptotic limit given by Eq. (60).

momentum distributions are shown in Fig. 12 at different bosonic concentrations x . We only report the case $\eta_B = 0$, since the effect of the BB repulsion is only limited to a slight renormalization of the Fermi step. We find a qualitatively analogous phenomenology to Fig. 11 even though the latter is obtained in the strong coupling limit of the theory. This is because the

effective interaction acting on fermions is given by an interplay between g and x , that is, even if g is strong, reducing x results in an effectively weaker g . In addition, we observe that the position of the Fermi step does not change significantly from weak to strong coupling, in contrast to the 3D case where the Fermi sphere is emptied by the vanishing of the Fermi wave vector [83]. In 2D, the destruction of the Fermi surface occurring with coupling or concentration takes place due to a strong renormalization of the fermionic quasi-particles, as described in Sec. III, and it is their weight rather than their associated Fermi momentum that vanishes.

Finally, in the inset, the fermionic momentum distribution is compared to the square modulus of the composite fermion wavefunction (60) in the large momentum limit where their ratio is expected to approach one.

C. Boson and fermion chemical potentials

We now discuss the results obtained for the Bose and Fermi chemical potentials. In the weak-coupling regime, one can expand the T -matrix in the small parameter $1/g$ and obtain analytical expressions for both chemical potentials. These calculations are carried out in detail in [93] and we only report the final results here

$$\mu_B = \frac{4\pi n_0 \eta_B}{m_B} + \frac{E_F}{g} \left[1 - \frac{1}{g} \left(\ln 2 - \frac{1}{2} \right) \right] \quad (58)$$

$$\mu_F = E_F + x \frac{E_F}{g} \left[1 + \frac{1}{g} (1 - \ln 2) \right]. \quad (59)$$

The first term in Eq. (58) arises from the standard Bogoliubov theory in 2D [91] whilst the second contribution stems from the BF interaction. One sees in Fig. 13 that in the weak-coupling regime, the numerical curves for both chemical potentials neatly approach the asymptotic limits (58,59) (dotted line on the left side). For the bosonic chemical potential this occurs in a universal way, i.e., independently of the value of x , as required by Eq. (58) which does not depend on the bosonic concentration (and ε_0 is exponentially suppressed in this regime). In the opposite regime, both chemical potentials approach their strong-coupling benchmarks, depicted by the dotted lines on the right side of the graph, which are seen to be strongly dependent on concentration. Note that, for the boson chemical potential, Fig. 13(a) reports the quantity $\mu_B + \varepsilon_0$, to subtract from the bosonic chemical potential the leading strong-coupling contribution, which is given by $-\varepsilon_0$, while the inset avoids this subtraction and illustrates on a logarithmic scale how the bosonic chemical potential tends to the binding energy, thus showing that all bosons are paired at large values of g .

Summing up, we find that two interaction regimes emerge from the above analysis: one for small g where barely dressed fermionic atoms are found along with weakly interacting bosons and varying the concentration has little effect, and one of large g in which, as x increases, the atomic assembly is strongly renormalized and experiences a collapse of the Fermi surface. The boundary between them can be roughly estimated

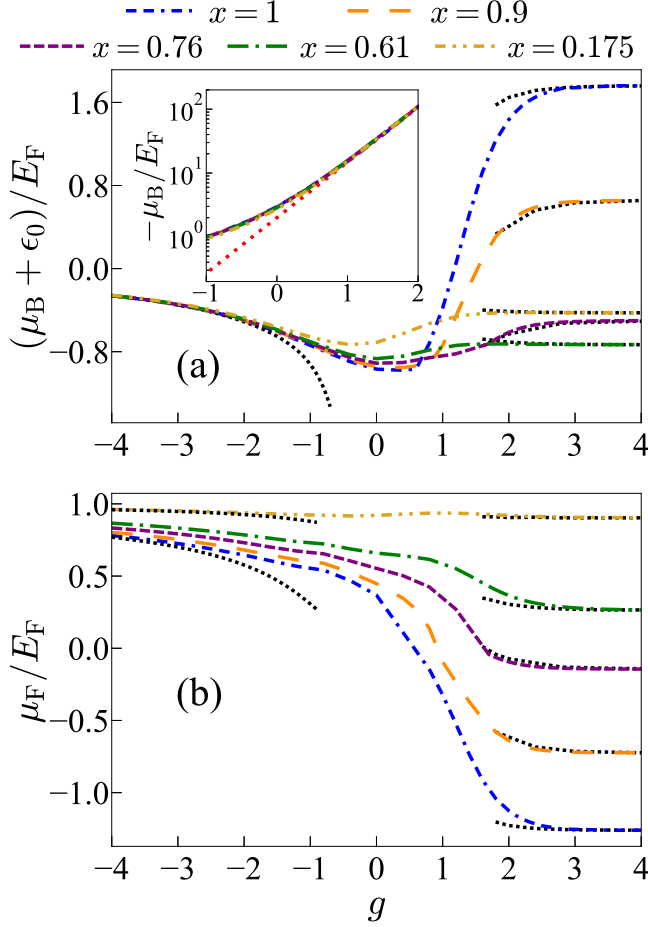


Figure 13. (a): Bosonic chemical potential μ_B (shifted by the binding energy ϵ_0) in units of the Fermi energy E_F as a function of the BF coupling g , for different values of bosonic concentration x at zero boson-boson repulsion $\eta_B = 0$. Dotted lines on the left: weak-coupling expression (58). Dotted lines on the right: strong coupling asymptotics of Sec. III. Inset: comparison between $-\mu_B/E_F$ and the binding energy ϵ_0/E_F (dotted line). (b): Corresponding fermionic chemical potential μ_F in units of the Fermi energy E_F . Dotted lines on the left: weak-coupling expression (59) (reported for clarity only for the two extreme values of x). Dotted lines on the right: strong coupling asymptotics of Sec. III.

by looking at the smallest coupling at which μ_F vanishes as a function of x and turns out to correspond to about $g \simeq 1$.

Finally, we note that we have verified that at finite $\eta_B = 0.1$ the results remain qualitatively the same, with quantitative changes affecting only μ_B , as also expected from the weak-coupling expression Eq. (58). The fermionic chemical potential is instead unaffected, in line with Eq. (59). On the other hand, in the strong coupling regime the boson-boson repulsion is essentially irrelevant due to the dominant dimer-atom repulsion.

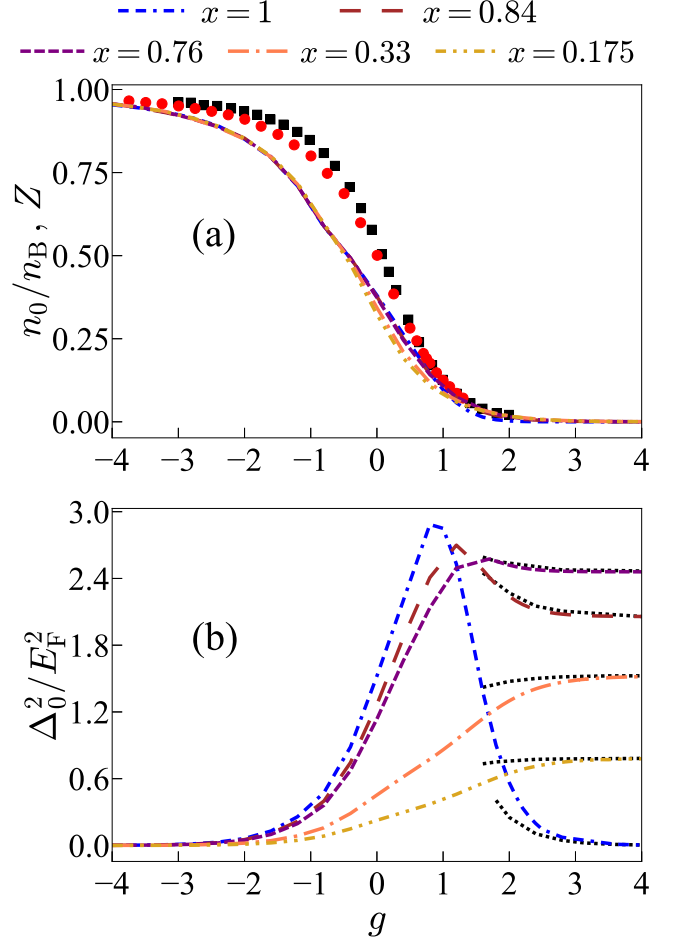


Figure 14. (a): Bosonic condensate fraction n_0/n_B as a function of the BF coupling parameter g , for different values of boson concentration x at zero BB repulsion $\eta_B = 0$. Circles: Diagrammatic Monte Carlo results for the polaron quasiparticle residue Z [105]. Squares: non-self-consistent T -matrix approximation results for the polaron quasiparticle residue Z [106]. (b): Square of hybridization energy scale Δ_0 (in units of E_F^2), as a function of the BF coupling g , for different values of the bosonic concentration x and boson-boson repulsion $\eta_B = 0$. Strong coupling benchmarks from Sec. III are also reported as dotted lines on the right.

D. Boson condensate density and atom-molecule hybridization energy scale

We now discuss the results for the bosonic condensate density n_0 and the related hybridization energy scale Δ_0 . Figure 14(a) reports the value of the condensate fraction as a function of coupling (for $\eta_B = 0$, without loss of generality for this quantity). A striking feature of Fig. 14(a) is the universal behavior of n_0 with respect to concentration, in complete analogy with what found in 3D [88] and recently confirmed experimentally in [33].

Figure 14(a) also reports the results for the polaron quasiparticle residue Z previously obtained with Diagrammatic Monte Carlo simulations (circles) [105] and within a non-

self-consistent T -matrix approach [106] (squares). This is because in 3D it was found [33, 88] that the universal condensate fraction essentially matches the quasiparticle residue Z of the Fermi polaron (which in our Bose-Fermi mixture corresponds to the limit of a single boson immersed in a Fermi gas).

Such identification between the universal condensate fraction and Z is challenged by the present results in 2D. One sees that, even though the condensate fraction n_0/n_B and the polaron quasiparticle residue Z share the same qualitative behavior, significant quantitative discrepancies between the two quantities are present. We emphasize that the existence of such a discrepancy cannot be ascribed to the specific choice of the self-energy used in our calculation. One sees indeed that such a discrepancy occurs also when Z is obtained with a non-self-consistent T -matrix approach (squares in Fig. 14(a)), which is exactly the same approach used here when carried over to the single-impurity limit. We thus conclude that the equivalence between the quasiparticle residue Z of the Fermi polaron and the universal condensate fraction observed in 3D is only approximate, and the differences between these two quantities are amplified in 2D.

A further difference with respect to the 3D case is observed in the behavior of n_0 for strong coupling. While in 3D n_0 drops identically to zero for values of g larger than a critical coupling g_c , in 2D n_0 never vanishes (even though it becomes exponentially small with the coupling g). This is because, as discussed in Sec. III D, the energy scale $\Delta_0 \propto (n_0 \varepsilon_0)^{1/2}$ has a non-negligible effect even when $n_0/n_B \approx 0$, if the boson and fermion populations are not exactly balanced. One sees indeed in Fig. 14(b) that Δ_0 vanishes only in the limit of balanced populations $x = 1$. Figure 14(b) also shows that the hybridization energy scale Δ_0 is almost negligible for small g whereas, for large g , Δ_0 saturates at values that depend on x . In this latter case, the maximum value is found at about $x \approx 0.7$ (short-dashed line) in line with the change of sign of μ_F in Fig. 13 and Fig. 3.

E. Tan's contact parameter and composite-fermion density

For large momenta the fermionic and bosonic distribution functions have the following asymptotic behaviors

$$n_F(k \gg k_F) = \frac{C_{BF}/4m_r^2}{\left(\frac{k^2}{2m_r} - \mu_B - \mu_F\right)^2}, \quad (60)$$

$$n_B(k \gg k_F) = \frac{C_{BF}/4m_r^2}{\left(\frac{k^2}{2m_r} - \mu_B - \mu_F\right)^2} + \frac{\Sigma_{12}^2}{4\left(\frac{k^2}{2m_B} - \mu_B\right)^2}, \quad (61)$$

whose leading order term, proportional to k^{-4} defines the Tan's contact parameter $C_s = n_s(k)k^4$, $s = F, B$, for fermions and bosons respectively [100–102]. The coefficient C_{BF} gives the contribution to the Tan's contacts due to BF pairing. Within our T -matrix self-energy approach, it can be shown to be given by

$$C_{BF} = 4m_r^2 \int \frac{d\mathbf{P}}{(2\pi)^2} \int \frac{d\Omega}{2\pi} T(\mathbf{P}, \Omega) e^{i\Omega 0^+} \quad (62)$$

similarly to what one obtains for analogous T -matrix approaches in the BCS-BEC crossover problem [107, 108].

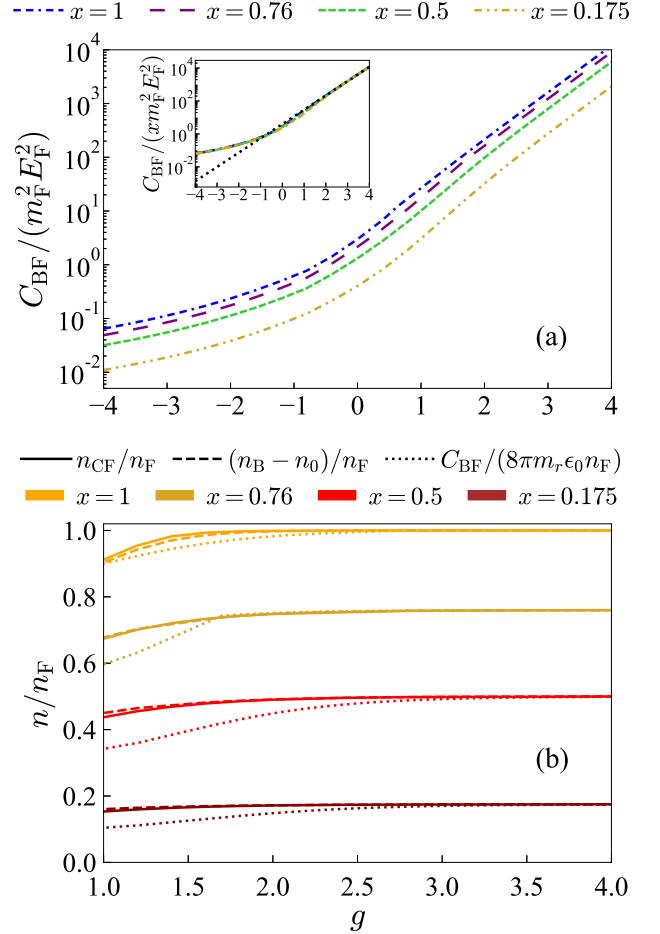


Figure 15. (a): Dimensionless Tan's contact constant $C_{BF}/m_F^2 E_F^2$ as a function of the BF coupling g , for different values of the bosonic concentration x at boson-boson repulsion $\eta_B = 0$. Inset: same data divided by the boson concentration x , compared with $2\varepsilon_0/E_F$ (dotted line). (b): Composite-fermion number density n_{CF} normalized to n_F (full lines), as obtained from Eq. (28) for different values of the bosonic concentration ($x = 1.0, 0.76, 0.5, 0.175$, from top to bottom) compared with $C_{BF}/(8\pi m_r \varepsilon_0 n_F)$ (dotted lines) and $(n_B - n_0)/n_F$ (dashed lines).

We show the results for C_{BF} of Eq. (62) in Fig. 15(a) from weak to strong BF attraction for different values of the bosonic concentration. The same quantity once divided by the boson density, C_{BF}/n_B , displays a universal behavior (see inset), in line with what already discussed for the condensate fraction (sec. IV D) and bosonic momentum distribution (sec. IV B). For this quantity, one sees that universality occurs for all couplings.

In the strong coupling regime, C_{BF} is seen in Fig. 15(a) to diverge exponentially with coupling. Specifically, as shown in the inset, the dimensionless quantity $C_{BF}/(m_F^2 E_F^2)$ scales like $2\varepsilon_0/E_F$ (dotted line in the inset), with the binding energy $\varepsilon_0/E_F = 2e^{2g}$. In this limit, once $T(\mathbf{P}, \Omega)$ is replaced in Eq.

(62) by $T_{\text{SC}}(\mathbf{P}, \Omega)$, one has indeed

$$\begin{aligned} C_{\text{BF}} &\approx 4m_r^2 \int \frac{d\mathbf{P}}{(2\pi)^2} \int \frac{d\Omega}{2\pi} T_{\text{SC}}(\mathbf{P}, \Omega) e^{i\Omega 0^+} \\ &= 8\pi m_r \varepsilon_0 \int \frac{d\mathbf{P}}{(2\pi)^2} \int \frac{d\Omega}{2\pi} G_{\text{CF}}(\mathbf{P}, \Omega) e^{i\Omega 0^+} \\ &= 8\pi m_r \varepsilon_0 n_{\text{CF}}, \end{aligned} \quad (63)$$

thus showing that in the strong coupling limit C_{BF} becomes proportional to the binding energy ε_0 multiplied by the density of BF pairs n_{CF} (where n_{CF} is defined by the strong-coupling expression (28)).

The presence of n_{CF} in Eq. (63) suggests comparing n_{CF} as defined by Eq. (28) and by expression $C_{\text{BF}}/(8\pi m_r \varepsilon_0 n_{\text{F}})$, in order to see when deviations from the asymptotic expression occur. This is done in Fig. 15(b) for several values of the concentration x (full lines and dotted lines, respectively). One sees that deviations are most significant at small concentrations, but for $g \gtrsim 2.5$ the contact essentially coincides with its asymptotic expressions for all cases. We notice furthermore that for $g \gtrsim 1$, the quantity n_{CF} essentially coincides with the number of bosons out of the condensate, $n_{\text{B}} - n_0$, (represented by the dashed lines in Fig. 15(b)). This justifies the assumption $n_{\text{CF}} \simeq n_{\text{B}} - n_0$ which we made in Sec. III D when discussing the strong-coupling limit of our theory.

F. Identification of different physical regions in the coupling-concentration plane

Based on the results obtained in Sec. III and Sec. IV B, the coupling ($g = -\ln(k_{\text{F}} a_{\text{BF}})$) vs. boson concentration ($x = n_{\text{B}}/n_{\text{F}}$) plane of a BF mixture can be divided in different physical region. Specifically, in Sec. III two different regimes were identified when varying the bosonic concentration for a fixed strong BF attraction. Analogously, two different regimes were identified in Sec. IV B when varying the coupling strength. Gathering all this information together, a schematic picture can be constructed as in Fig. 16, whereby a number of different physical regimes are detected:

- *Weakly interacting BF mixture:* a majority of weakly perturbed Fermi atoms coexists with a mildly depleted bosonic condensate; bosons out of the condensate marginally engage in molecule formation;
- *Strongly interacting BF mixture:* Fermi atoms are strongly paired with bosonic atoms, resulting in a significant depletion of the condensate, which in turn mediates a strong hybridization of molecular BF states with unpaired atomic ones;
- *Hybridized Fermi-Fermi mixture:* the condensate is almost fully depleted and bosons are fully paired up in molecules; a residual condensate density supports the hybridization of unpaired fermionic states with molecular states;
- *Non-interacting molecular gas:* Fermi molecules are the majority species; the hybridizing effect of the residual

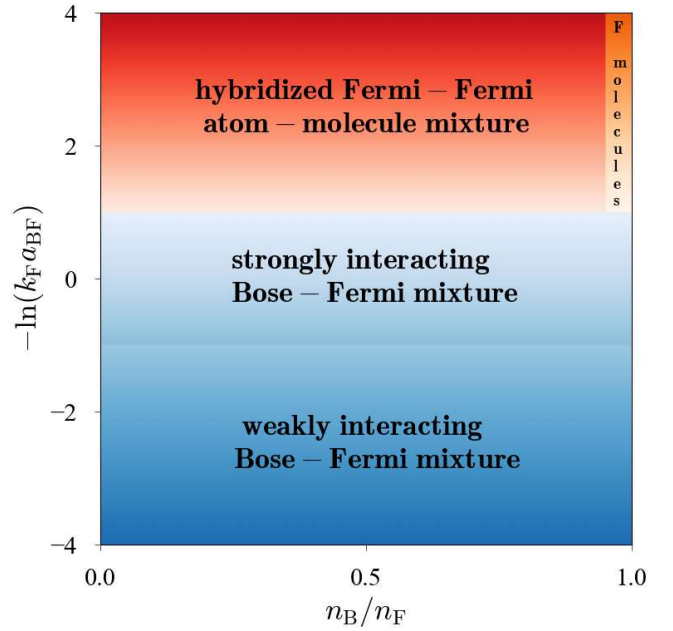


Figure 16. Schematic subdivision of the coupling vs. boson concentration plane of an attractive Bose-Fermi mixture in different physical regions.

condensate vanishes, leaving a gas of non-interacting pure molecules.

V. CONCLUSIONS AND OUTLOOK

In this work, we have analyzed the competition between boson condensation and BF pairing in 2D Bose-Fermi mixtures with an attractive and tunable BF interaction, extending previous work for the 3D case. We focused on the case with concentration of bosons $x = n_{\text{F}}/n_{\text{B}} \leq 1$, allowing for a full competition between pairing and condensation.

We have described analogies and differences with respect to the 3D case. Specifically, we have found that, like in 3D, the condensate is progressively depleted as the BF attraction increases and molecular correlations set in. However, in 2D the condensate never vanishes, but rather becomes exponentially small for large BF attractions. This marks a difference with respect to 3D, where the condensate was found to vanish beyond a critical coupling strength.

Similarly to the 3D case, we uncovered a nearly universal behavior for the condensate fraction and bosonic momentum distribution with respect to the boson concentration. Contrary to the 3D case, however, we have found that the universal condensate fraction does not match the quasiparticle residue Z of the Fermi polaron. It would be interesting to understand whether the equivalence between these two quantities observed in 3D has an intrinsic explanation or is simply an accidental degeneracy that is removed in 2D.

A further difference with respect to the 3D case is the hybrid nature of the composite fermions that form for sufficiently

strong BF attraction, with associated rather unusual momentum distributions, except for the case $x = 1$ in which the mixture “fermionizes” completely in a gas of non-interacting point-like fermionic molecules, similarly to what is obtained in 3D for all $x \leq 1$. The origin of this difference for $x < 1$ is in the residual condensate density n_0 which, albeit small, proves sufficient to generate a significant hybridization through the hybridization energy-scale $\Delta_0 \propto (n_0 \varepsilon_0)^{1/2}$.

A discussion on possible refinements of the present approach is finally in order. The absence of a quantum phase transition for the condensate fraction found in the present work, recalls the absence of the polaron-to-molecule transition that is found in the single impurity limit of a Fermi polaron, when the polaron is described by a non-self-consistent T -matrix self-energy [109]. In this limit, it has been pointed out that a correct description of the atom-dimer interaction is crucial in bringing about this transition [109, 110].

In Sec. III A and Sec. III B, we mentioned that the non-self-consistent T -matrix approximation takes into account the atom-dimer interaction at the level of the Born approximation, resulting in coupling-independent mean-field shifts Σ_{CF} and Σ_F^0 . While in 3D the Born approximation is qualitatively correct, in 2D these Hartree-like contributions definitely overestimate the effective repulsion between molecules and unpaired fermionic atoms, making the molecular state energetically less convenient, and favoring a state in which the molecule hybridizes with an unpaired state made of a fermionic atom and a boson belonging to the condensate. In order to go beyond the Born approximation, one should, in principle, include in a many-body theory the same kind of diagrams (involving two fermions repeatedly exchanging a boson) describing the atom-dimer scattering in the three-body problem [97, 111, 112] (see also [113]), a task that is far from trivial.

Insight from the polaron limit may suggest that the absence of a critical coupling strength in 2D is simply an artifact of the approximation for the self-energy here adopted. We do not exclude such a possibility. We however stress that, in experiments, the exponential vanishing of the condensate at large coupling strength, which we have found in the present work, would hardly be distinguishable from an exact vanishing of the condensate (leaving aside the fact that at finite temperature, as experimentally relevant, one should consider a quasi-condensate in 2D, introducing a further source of smearing of the transition).

Further on this point, recent work [87] has illustrated the relevance of three-body correlations in addressing the polaron-molecule quantum phase transition via an effective field theory approach based on a gradient expansion of the T -matrix for small momenta and frequencies and neglecting the condensation of bosons. In the present approach, we consider the full dependence of the T -matrix on momenta and frequencies in the presence of a Bose condensate, thus being able to span the full range of concentrations from a single impurity to equal densities. In particular, in the case $n_B = n_F$, three-body processes are expected to be negligible, making our results less sensitive to these diagrammatic contributions.

Finally, it is worth pointing out that, since the polaron-to-molecule quantum phase transition is proven to occur specifi-

cally in the impurity limit, one may expect that in the high concentration regime, where the polaron picture breaks down, this transition could be suppressed or significantly modified by quantum fluctuations. It is known in 3D [33, 114] that, with a finite density of impurities, thermal and quantum fluctuations smoothens the discontinuity arising in the single impurity limit thus shifting the critical coupling to higher values. An analogous and stronger role may be played by quantum fluctuations in 2D. To settle this point, a detailed calculation of the three-body diagrammatic contributions for finite densities beyond the polaronic regime, should be addressed in future work.

ACKNOWLEDGMENTS

We thank Dr. Andrea Guidini for contributing in an early stage of this work. We acknowledge the use of computational resources from the parallel computing cluster of the Open Physics Hub at the Physics and Astronomy Department in Bologna. Financial support from the Italian Ministry of University and Research under project PRIN2022, Contract No. 2022523NA7 and from the European Union - NextGenerationEU through the Italian Ministry of University and Research under PNRR - M4C2 - I1.4 Contract No. CN00000013 is also acknowledged.

Appendix A: Normal phase T -matrix $\Gamma(\mathbf{P}, \Omega)$

Evaluating the integral over ω in Eq. (3) on the complex plane by closing the contour on the left-hand side and rearranging the terms of the resulting geometric series, one obtains

$$\Gamma(\mathbf{P}, \Omega)^{-1} = \frac{1}{v_0^{\text{BF}}} + \int \frac{d\mathbf{k}}{(2\pi)^2} \frac{1 - \Theta(-\xi_{\mathbf{P}-\mathbf{k}}^{\text{F}}) - \Theta(-\xi_{\mathbf{k}}^{\text{B}})}{\xi_{\mathbf{P}-\mathbf{k}}^{\text{F}} + \xi_{\mathbf{k}}^{\text{B}} - i\Omega}, \quad (\text{A1})$$

whereby the Θ functions appearing in the integrand descend from the Fermi and Bose distributions in the zero temperature limit. In particular, for the coupling strengths and concentrations considered in this work, μ_B is always negative, hence $\Theta(-\xi_{\mathbf{k}}^{\text{B}}) = 0$.

The ultraviolet divergence in the integral of Eq. (A1) is regularized by expressing v_0^{BF} in terms of the boson-fermion binding energy ε_0 of the two-body problem in vacuum as in Eq. (2), thus yielding

$$\Gamma(\mathbf{P}, \Omega)^{-1} = T_2(\mathbf{P}, \Omega)^{-1} - I_{\text{F}}(\mathbf{P}, \Omega), \quad (\text{A2})$$

where T_2 is the off-shell two-body T -matrix in vacuum [93], which for $\Omega \neq 0$ is given by

$$\begin{aligned} T_2(\mathbf{P}, \Omega)^{-1} &= \frac{1}{v_0^{\text{BF}}} + \int \frac{d\mathbf{k}}{(2\pi)^2} \frac{1}{\xi_{\mathbf{P}-\mathbf{k}}^{\text{F}} + \xi_{\mathbf{k}}^{\text{B}} - i\Omega} \\ &= -\frac{m_r}{2\pi} \ln \left(\frac{\frac{P^2}{2M} - \mu_{\text{F}} - \mu_{\text{B}} - i\Omega}{\varepsilon_0} \right). \end{aligned} \quad (\text{A3})$$

The contribution $I_F(\mathbf{P}, \Omega)$ stems from the presence of a

degenerate fermionic component

$$I_F(\mathbf{P}, \Omega) = \int \frac{d\mathbf{k}}{(2\pi)^2} \frac{\Theta(-\xi_{\mathbf{P}-\mathbf{k}}^F)}{\xi_{\mathbf{P}-\mathbf{k}}^F + \xi_{\mathbf{k}}^B - i\Omega}, \quad (\text{A4})$$

therefore it is absent if $\mu_F \leq 0$.

For $\mu_F > 0$ Eq. (A4) can be expressed in closed form as follows (with $\Omega \neq 0$)

$$I_F(\mathbf{P}, \Omega) = \frac{m_r}{2\pi} \begin{cases} \ln \frac{\mathcal{A}}{\alpha + \beta} & \text{for } \mu_F + \mu_B \leq \frac{P^2}{2m_B}; \\ \ln \frac{\mathcal{A}(\alpha - \beta)}{\mathcal{B}^2} + i\pi \text{sgn}(\Omega) & \text{for } \mu_F + \mu_B > \frac{P^2}{2m_B} \text{ and } k_+ \leq k_{\mu_F}; \\ -\ln \frac{\mathcal{A}}{\alpha - \beta} + i\pi \text{sgn}(\Omega) & \text{for } \mu_F + \mu_B > \frac{P^2}{2m_B} \text{ and } k_+ > k_{\mu_F}, \end{cases}$$

where

$$\mathcal{A} = \beta + \frac{k_{\mu_F}^2}{2m_r} + \sqrt{\alpha^2 + \beta \frac{k_{\mu_F}^2}{m_r} + \frac{k_{\mu_F}^4}{4m_r^2}}, \quad (\text{A5})$$

$$\mathcal{B}^2 = \left(i\Omega + \frac{P^2}{m_B^2} m_r \right)^2 + \frac{P^2}{m_B^2} k_+^2 + \Omega^2, \quad (\text{A6})$$

and

$$\begin{aligned} \frac{k_+^2}{2m_r} &= \mu_F + \mu_B - \frac{P^2}{2m_B}, & \frac{k_{\mu_F}^2}{2m_F} &= \mu_F, \\ \alpha &= -\frac{k_+^2}{2m_r} - i\Omega, & \beta &= \alpha - \frac{P^2}{m_B^2} m_r. \end{aligned}$$

Appendix B: 3-body T -matrix in 2D vacuum within Born approximation

We briefly illustrate the evaluation of the 3-body T -matrix within Born approximation in the 2D vacuum. We start by recalling the Skorniakov-Ter-Martirosian equation for the 3-body T -matrix $T_3(k, p; K)$ describing the scattering between a BF dimer and a fermionic atom of initial three-momenta $K - k$ and k and final three-momenta $K - p$ and p , respectively [111, 115]:

$$\begin{aligned} T_3(k, p; K) &= -G_B^0(K - k - p) \\ &- \int \frac{d\mathbf{q}}{(2\pi)^2} \frac{dq_0}{(2\pi)} G_B^0(K - k - q) G_F^0(q) T_2(K - q) T_3(q, p; K), \end{aligned} \quad (\text{B1})$$

where we have introduced the three-vector notation $q = (\mathbf{q}, q_0)$, where q_0 is a frequency, and G_B^0 and G_F^0 are the Bose and Fermi Green's function in vacuum

$$G_s^0(q) = \frac{1}{q_0 - \mathbf{q}^2/2m_s + i0^+} \quad s = \text{B, F}. \quad (\text{B2})$$

Within Born approximation, T_3 is replaced with the first term on the right-hand side of Eq. B1. Moreover, for low energy scattering one can set $k_1 \simeq k_2 \simeq 0$ and $K \equiv \{\mathbf{0}, -\varepsilon_0\}$, (taking into account the binding energy ε_0 of the BF dimer). Recalling that T_2 is a dimer propagator except for the form factor $2\pi\varepsilon_0/m_r$ (see Eq. 19) due to its composite nature, the same normalization factor is applied to T_3 , which thus becomes independent of the two-body scattering length a_{BF}

$$\frac{2\pi\varepsilon_0}{m_r} T_3(0, 0; \{\mathbf{0}, -\varepsilon_0\}) \simeq -\frac{2\pi\varepsilon_0}{m_r} G_B^0(\mathbf{0}, -\varepsilon_0) = \frac{2\pi}{m_r}. \quad (\text{B3})$$

Appendix C: Convergence of numerical integrals

The convergence of the frequency integrals appearing in expressions (10), (11), (14) and (15) is guaranteed by the presence of the causality factors $e^{i\Omega 0^+}$ and $e^{i\omega 0^+}$ but in an extremely slow fashion. In order to avoid this problem altogether, we add to and subtract from the integrand an analytically integrable auxiliary function with the same asymptotic behavior. By doing so, the integral turns out to be absolutely convergent and can be calculated numerically up to a high-frequency cutoff. Beyond the latter, the integration is performed analytically when computing the self-energies (10)-(11) and the contact parameter (62), whereas it is neglected in the case of momentum distributions (14)-(15). The formulas presented in the next subsections illustrate these two different cases. The remaining integral of the added auxiliary function can be instead integrated analytically thanks to the convergence factor.

1. Self-energies

Starting from the self-energy for bosons (8), we recast it as follows

$$\begin{aligned} \Sigma_{\text{BF}} = & \int \frac{d\mathbf{P}}{(2\pi)^2} \int_{-\infty}^{\infty} \frac{d\Omega}{2\pi} [T(\mathbf{P}, \Omega) G_{\text{F}}^0(\mathbf{P} - \mathbf{k}, \Omega - \omega) \\ & - \Gamma_{\text{SC}}(\mathbf{P}, \Omega) G_{\text{F}}^{00}(\mathbf{P} - \mathbf{k}, \Omega - \omega)] \\ & + \int \frac{d\mathbf{P}}{(2\pi)^2} \int_{-\infty}^{\infty} \frac{d\Omega}{2\pi} \Gamma_{\text{SC}}(\mathbf{P}, \Omega) G_{\text{F}}^{00}(\mathbf{P} - \mathbf{k}, \Omega - \omega) e^{i\Omega 0^+}, \end{aligned} \quad (\text{C1})$$

where G_{F}^{00} is a bare fermionic Green's function with $\mu_{\text{F}}^0 = 0^-$. The second frequency integral is evaluated via contour integration closing on the left-hand side and contributing with a pole and a branch cut when they fall in this region. Instead, the first frequency integration is split in three regions: $[-\infty, -\Omega_c] \cup [-\Omega_c, \Omega_c] \cup [\Omega_c, \infty]$. For $|\Omega| \geq \Omega_c$ the integral is carried out analytically exploiting the subleading asymptotic expression of the integrand. The remaining frequency range is instead treated numerically.

Regarding integration in momentum space, the angular integral can be carried out analytically, since the dependence on the angle appears only in the bare Green's function. Finally, radial integrals are evaluated numerically up to a natural cut-off given by the position of the highest Fermi step in the integrand function. In particular, we find one step arising from the pole of the T -matrix and up to two steps coming from the poles of the fermionic Green's function.

The calculations for the fermionic self-energy Σ_{F} follow the same approach as above provided G_{F}^{00} and G_{F}^0 are replaced with G_{B}^0 . Since the bosonic bare Green's function does not have a pole, the final momentum integration is carried out simply over a single finite interval.

2. Momentum distributions and densities

The momentum distributions Eqs. (14)-(15) are given by

$$\begin{aligned} n_{\text{F}}(\mathbf{k}) &= \int_{-\infty}^{\infty} \frac{d\omega}{2\pi} G_{\text{F}}(\mathbf{k}, \omega) e^{i\omega 0^+} \\ &\simeq 2 \int_0^{\omega_c} \frac{d\omega}{2\pi} \text{Re} [G_{\text{F}}(\mathbf{k}, \omega) - G_{\text{F}}^0(\mathbf{k}, \omega)] + \Theta(-\xi_{\mathbf{k}}^{\text{F}}), \quad (\text{C2}) \\ n_{\text{B}}(\mathbf{k}) &= \int_{-\infty}^{\infty} \frac{d\omega}{2\pi} G_{\text{B}}(\mathbf{k}, \omega) e^{i\omega 0^+} \\ &\simeq 2 \int_0^{\omega_c} \frac{d\omega}{2\pi} \text{Re} [G_{\text{B}}(\mathbf{k}, \omega) - G_{\text{B}}^{0'}(\mathbf{k}, \omega)] \\ &\quad + \frac{1}{2} \left[\frac{\xi_{\mathbf{k}}^{\text{B}} + \Sigma_{11}}{\sqrt{(\xi_{\mathbf{k}}^{\text{B}} + \Sigma_{11})^2 - \Sigma_{12}^2}} - 1 \right], \quad (\text{C3}) \end{aligned}$$

where the bosonic Green's function in the Bogoliubov approximation is given by

$$G_{\text{B}}^{0'}(\mathbf{k}, \omega) = \left(i\omega - \xi_{\mathbf{k}}^{\text{B}} - \Sigma_{11} + \frac{\Sigma_{12}^2}{i\omega + \xi_{\mathbf{k}}^{\text{B}} + \Sigma_{11}} \right)^{-1}. \quad (\text{C4})$$

The frequency cutoff ω_c is set to $50000E_{\text{F}}$ so to make the contribution of the integrands negligible for $\omega \geq \omega_c$, whereas in the range $100E_{\text{F}} \leq \omega \leq \omega_c$ the following asymptotic formulas are exploited for the self-energies appearing in the above Green's functions

$$\Sigma_{\text{F}}(\mathbf{k}, \omega) \xrightarrow{\omega \rightarrow \infty} n_0 \Gamma(\mathbf{k}, \omega) - \left(\frac{C_{\text{BF}}}{4m_r^2} \right) G_{\text{B}}^0(\mathbf{k}, -\omega), \quad (\text{C5})$$

$$\Sigma_{\text{B}}(\mathbf{k}, \omega) \xrightarrow{\omega \rightarrow \infty} \Sigma_{11} + n_{\mu_{\text{F}}} T(\mathbf{k}, \omega) - \left(\frac{C_{\text{BF}}}{4m_r^2} \right) G_{\text{F}}^0(\mathbf{k}, -\omega) \quad (\text{C6})$$

The last terms in Eq. (C2) and in Eq. (C3) originate from the frequency integration of the added and subtracted Green's functions, $G_{\text{F}}^0(\mathbf{k}, \omega)$ and $G_{\text{B}}^{0'}(\mathbf{k}, \omega)$ respectively.

One then arrives at the densities

$$\begin{aligned} n_{\text{F}} &= \int_0^{\infty} \frac{dk}{2\pi} k n_{\text{F}}(k) \\ &= \int_0^{k_c} \frac{dk}{2\pi} k n_{\text{F}}(k) + \frac{\frac{C_{\text{BF}}}{4m_r}}{2\pi \left(\frac{k_c^2}{2m_r} - \mu_{\text{B}} - \mu_{\text{F}} \right)}, \quad (\text{C7}) \end{aligned}$$

$$\begin{aligned} n_{\text{B}} &= n_0 + \int_0^{\infty} \frac{dk}{2\pi} k n_{\text{B}}(k) = n_0 + \int_0^{k_c} \frac{dk}{2\pi} k n_{\text{B}}(k) \\ &\quad + \frac{\frac{C_{\text{BF}}}{4m_r}}{2\pi \left(\frac{k_c^2}{2m_r} - \mu_{\text{B}} - \mu_{\text{F}} \right)} + \frac{m_{\text{B}} \Sigma_{12}^2}{8\pi \left(\frac{k_c^2}{2m_{\text{B}}} - \mu_{\text{B}} \right)}, \quad (\text{C8}) \end{aligned}$$

where we have used the asymptotic expressions (60)-(61).

3. BF contact parameter C_{BF}

The BF pairing contribution C_{BF} to the Tan's contact parameter is proportional to the trace of the T -matrix [107], which is recast as follows

$$\begin{aligned} \frac{C_{\text{BF}}}{4m_r^2} &= \int \frac{d\mathbf{P}}{(2\pi)^2} \int_{-\infty}^{\infty} \frac{d\Omega}{2\pi} T(\mathbf{P}, \Omega) e^{i\Omega 0^+} \quad (\text{C9}) \\ &= \int \frac{d\mathbf{P}}{(2\pi)^2} \int_{-\infty}^{\infty} \frac{d\Omega}{2\pi} [T(\mathbf{P}, \Omega) - \Gamma^{\text{SC}}(\mathbf{P}, \Omega)] + \\ &\quad \int \frac{d\mathbf{P}}{(2\pi)^2} \int_{-\infty}^{\infty} \frac{d\Omega}{2\pi} \Gamma_{\text{SC}}(\mathbf{P}, \Omega) e^{i\Omega 0^+} \quad (\text{C10}) \\ &= \int \frac{d\mathbf{P}}{(2\pi)^2} \left\{ 2\text{Re} \left[\int_0^{\Omega_c} \frac{d\Omega}{2\pi} [T(\mathbf{P}, \Omega) - \Gamma_{\text{SC}}(\mathbf{P}, \Omega)] + \right. \right. \\ &\quad \left. \left. \frac{2\pi (n_0 + n_{\mu_{\text{F}}}) \pi/2 - i (\ln \Omega_c - \ln \varepsilon_0)}{m_r^2 \pi^2/4 + \ln^2 \Omega_c - \ln^2 \varepsilon_0} \right] + \right. \\ &\quad \left. \frac{2\pi}{m_r} \left[\varepsilon_0 \Theta(-\xi_{\mathbf{P}}^{\text{CF}}) + \Theta(-z_c) \int_{z_c}^0 \frac{dx}{\ln^2(x - z_c) - \ln^2 \varepsilon_0 + \pi^2} \right] \right\} \quad (\text{C11}) \end{aligned}$$

where Ω_c is the high-frequency cutoff, the term in the second line of Eq. (C11) comes from the analytical integration of the asymptotic form of $T(\mathbf{P}, \Omega) - \Gamma_{\text{SC}}(\mathbf{P}, \Omega)$ in the range $[\Omega_c, +\infty]$ with the definition $n_{\mu_F} = 2m_F\mu_F\Theta(\mu_F)$, whereas in the last line $z_c = P^2/2M - \mu_B - \mu_F$ and $\xi_{\mathbf{P}}^{\text{CF}} = P^2/2M - \mu_{\text{CF}}$. The remaining integrations over Ω , x and P are evaluated numerically.

Appendix D: Analytic evaluations in the strong-coupling limit

The integral in expression (28) can be computed analytically and is given in closed form as

$$\begin{aligned} \frac{n_{\text{CF}}}{n_F} = & \Theta(y_+) \left[\frac{y_+}{2} - \sqrt{4\bar{\Delta}_0^2 + \left(\bar{\mu}_{\text{CF}} - \bar{\mu}_F + \frac{y_+}{2}\right)^2} \right. \\ & \left. + \sqrt{4\bar{\Delta}_0^2 + \left(\bar{\mu}_{\text{CF}} - \bar{\mu}_F\right)^2} \right] \\ & + \Theta(y_-) \left[\frac{y_-}{2} + \sqrt{4\bar{\Delta}_0^2 + \left(\bar{\mu}_{\text{CF}} - \bar{\mu}_F + \frac{y_-}{2}\right)^2} \right. \\ & \left. - \sqrt{4\bar{\Delta}_0^2 + \left(\bar{\mu}_{\text{CF}} - \bar{\mu}_F\right)^2} \right], \end{aligned} \quad (\text{D1})$$

with y_{\pm} solutions of the equations

$$\bar{\xi}_y^{\text{CF}} + \bar{\xi}_y^{\text{F}} \pm \sqrt{(\bar{\xi}_y^{\text{CF}} - \bar{\xi}_y^{\text{F}})^2 + 4\bar{\Delta}_0^2} = 0, \quad (\text{D2})$$

where $\bar{\xi}_y^{\text{CF}} = m_F y / M - \bar{\mu}_{\text{CF}}$ and $\bar{\xi}_y^{\text{F}} = y - \bar{\mu}_F$, and all quantities with a bar on top are in units of E_F .

The Hugenholtz-Pines condition (52) can be evaluated ana-

lytically and, in terms of the quantity

$$I_{\pm}(y) = \ln \left[\sqrt{4\bar{\Delta}_0^2 + \left(\bar{\mu}_{\text{CF}} - \bar{\mu}_F + \frac{y}{2}\right)^2} \pm \left(\bar{\mu}_{\text{CF}} - \bar{\mu}_F + \frac{y}{2}\right) \right], \quad (\text{D3})$$

reads

$$\mu_B = -4\varepsilon_0 \left\{ [I_-(y_+) - I_-(0)]\Theta(y_+) + [I_+(y_-) - I_+(0)]\Theta(y_-) \right\} \quad (\text{D4})$$

with y_+ and y_- defined as in Eq. D1.

In the special case $x = 1$ and for $g \rightarrow \infty$, $\Delta_0 \rightarrow 0$ (as shown in Fig. 14) and the above expression acquires the simplified and recursive form

$$\mu_B = -4\varepsilon_0 \ln \left[1 + \frac{\mu_{\text{CF}}}{\mu_B + \varepsilon_0} \right], \quad (\text{D5})$$

where $\bar{\mu}_{\text{CF}} = \mu_{\text{CF}}$ since $\Sigma_{\text{CF}} = 0$ and the definition $\mu_{\text{CF}} = \mu_F + \mu_B + \varepsilon_0$ has been used.

With the replacement $t \equiv (\mu_B + \varepsilon_0)/\mu_{\text{CF}}$ it holds that $\mu_B/\varepsilon_0 = t\mu_{\text{CF}}/\varepsilon_0 - 1$. To leading order in the small parameter $\mu_{\text{CF}}/\varepsilon_0$, Eq. D5 reduces to $\frac{1}{4} = \ln \left[1 + \frac{1}{t} \right]$, with solution

$$t \equiv \frac{\mu_B + \varepsilon_0}{\mu_{\text{CF}}} = \frac{1}{e^{\frac{1}{4}} - 1}. \quad (\text{D6})$$

For balanced populations all bosons are expected to bind with fermions into pairs which implies that $n_0 = 0$ and, since $n_{\text{CF}} = n_F$, it must hold that $\mu_{\text{CF}} = E_F/2$ (as one can verify using expression (28)) allowing us to analytically determine the values of both the fermionic and bosonic chemical potentials through Eq. (D6):

$$\mu_B = -\varepsilon_0 + \frac{1}{e^{\frac{1}{4}} - 1} \frac{E_F}{2} \quad (\text{D7})$$

$$\mu_F = \frac{e^{\frac{1}{4}} - 2}{e^{\frac{1}{4}} - 1} \frac{E_F}{2}. \quad (\text{D8})$$

-
- [1] Kenji Maeda, Gordon Baym, and Tetsuo Hatsuda, ‘‘Simulating Dense QCD Matter with Ultracold Atomic Boson-Fermion Mixtures,’’ *Phys. Rev. Lett.* **103**, 085301 (2009).
 - [2] F. Iachello and P. van Isacker, *The interacting boson-fermion model* (Cambridge University Press, 1991).
 - [3] Gordon Baym and Christopher Pethick, *Landau Fermi-Liquid Theory* (Wiley-VCH Publications, 2004).
 - [4] G. R. Stewart, ‘‘Unconventional superconductivity,’’ *Advances in Physics* **66**, 75–196 (2017).
 - [5] Ehud Altman, Kenneth R. Brown, Giuseppe Carleo, Lincoln D. Carr, Eugene Demler, Cheng Chin, Brian DeMarco, Sophia E. Economou, Mark A. Eriksson, Kai-Mei C. Fu, Markus Greiner, Kaden R.A. Hazzard, Randall G. Hulet, Alicia J. Kollár, Benjamin L. Lev, Mikhail D. Lukin, Ruichao Ma, Xiao Mi, Shashank Misra, Christopher Monroe, Kater Murch, Zaira Nazario, Kang-Kuen Ni, Andrew C. Potter, Pedram Roushan, Mark Saffman, Monika Schleier-Smith, Irfan Siddiqi, Raymond Simmonds, Meenakshi Singh, I.B. Spielman, Kristan Temme, David S. Weiss, Jelena Vučković, Vladan Vuletić, Jun Ye, and Martin Zwierlein, ‘‘Quantum Simulators: Architectures and Opportunities,’’ *PRX Quantum* **2**, 017003 (2021).
 - [6] K.-K. Ni, S. Ospelkaus, M. H. G. de Miranda, A. Pe’er, B. Neyenhuis, J. J. Zirbel, S. Kotochigova, P. S. Julienne, D. S. Jin, and J. Ye, ‘‘A High Phase-Space-Density Gas of Polar Molecules,’’ *Science* **322**, 231–235 (2008).
 - [7] Cheng-Hsun Wu, Ibon Santiago, Jee Woo Park, Peyman Ahmadi, and Martin W. Zwierlein, ‘‘Strongly interacting isotopic Bose-Fermi mixture immersed in a Fermi sea,’’ *Phys. Rev. A* **84**, 011601 (2011).
 - [8] Cheng-Hsun Wu, Jee Woo Park, Peyman Ahmadi, Sebastian Will, and Martin W. Zwierlein, ‘‘Ultracold Fermionic Feshbach Molecules of $^{23}\text{Na}^{40}\text{K}$,’’ *Phys. Rev. Lett.* **109**, 085301 (2012).
 - [9] Jee Woo Park, Cheng-Hsun Wu, Ibon Santiago, Tobias G. Tiecke, Sebastian Will, Peyman Ahmadi, and Martin W. Zwierlein, ‘‘Quantum degenerate Bose-Fermi mixture of chemically different atomic species with widely tunable interac-

- tions,” *Phys. Rev. A* **85**, 051602 (2012).
- [10] Myoung-Sun Heo, Tout T. Wang, Caleb A. Christensen, Timur M. Rvachov, Dylan A. Cotta, Jae-Hoon Choi, Ye-Ryoung Lee, and Wolfgang Ketterle, “Formation of ultracold fermionic NaLi Feshbach molecules,” *Phys. Rev. A* **86**, 021602 (2012).
- [11] Tyler D. Cumby, Ruth A. Shewmon, Ming-Guang Hu, John D. Perreault, and Deborah S. Jin, “Feshbach-molecule formation in a Bose-Fermi mixture,” *Phys. Rev. A* **87**, 012703 (2013).
- [12] Ruth S. Bloom, Ming-Guang Hu, Tyler D. Cumby, and Deborah S. Jin, “Tests of Universal Three-Body Physics in an Ultracold Bose-Fermi Mixture,” *Phys. Rev. Lett.* **111**, 105301 (2013).
- [13] Pietro Massignan, Matteo Zaccanti, and Georg M Bruun, “Polarons, dressed molecules and itinerant ferromagnetism in ultracold Fermi gases,” *Reports on Progress in Physics* **77**, 034401 (2014).
- [14] V. D. Vaidya, J. Tiamsuphat, S. L. Rolston, and J. V. Porto, “Degenerate Bose-Fermi mixtures of rubidium and ytterbium,” *Phys. Rev. A* **92**, 043604 (2015).
- [15] I. Ferrier-Barbut, M. DeLahaye, S. Laurent, A. T. Grier, M. Pierce, B. S. Rem, F. Chevy, and C. Salomon, “A mixture of Bose and Fermi superfluids,” *Science* **345**, 1035–1038 (2014).
- [16] Marion DeLahaye, Sébastien Laurent, Igor Ferrier-Barbut, Shuwei Jin, Frédéric Chevy, and Christophe Salomon, “Critical Velocity and Dissipation of an Ultracold Bose-Fermi Counterflow,” *Phys. Rev. Lett.* **115**, 265303 (2015).
- [17] Ming-Guang Hu, Michael J. Van de Graaff, Dhruv Kedar, John P. Corson, Eric A. Cornell, and Deborah S. Jin, “Bose Polarons in the Strongly Interacting Regime,” *Phys. Rev. Lett.* **117**, 055301 (2016).
- [18] Yu-Ping Wu, Xing-Can Yao, Hao-Ze Chen, Xiang-Pei Liu, Xiao-Qiong Wang, Yu-Ao Chen, and Jian-Wei Pan, “A quantum degenerate Bose-Fermi mixture of 41K and 6Li,” *J. Phys. B At. Mol. Opt. Phys.* **50**, 094001 (2017).
- [19] Richard Roy, Alaina Green, Ryan Bowler, and Subhadeep Gupta, “Two-Element Mixture of Bose and Fermi Superfluids,” *Phys. Rev. Lett.* **118**, 055301 (2017).
- [20] Yu-Ping Wu, Xing-Can Yao, Xiang-Pei Liu, Xiao-Qiong Wang, Yu-Xuan Wang, Hao-Ze Chen, Youjin Deng, Yu-Ao Chen, and Jian-Wei Pan, “Coupled dipole oscillations of a mass-imbalanced Bose-Fermi superfluid mixture,” *Phys. Rev. B* **97**, 020506 (2018).
- [21] A. Trautmann, P. Ilzhöfer, G. Durastante, C. Politi, M. Sohmen, M. J. Mark, and F. Ferlaino, “Dipolar Quantum Mixtures of Erbium and Dysprosium Atoms,” *Phys. Rev. Lett.* **121**, 213601 (2018).
- [22] Rianne S. Lous, Isabella Fritsche, Michael Jag, Fabian Lehmann, Emil Kirilov, Bo Huang, and Rudolf Grimm, “Probing the Interface of a Phase-Separated State in a Repulsive Bose-Fermi Mixture,” *Phys. Rev. Lett.* **120**, 243403 (2018).
- [23] Richard Schmidt, Michael Knap, Dmitri A Ivanov, Jih-Shih You, Marko Cetina, and Eugene Demler, “Universal many-body response of heavy impurities coupled to a Fermi sea: a review of recent progress,” *Reports on Progress in Physics* **81**, 024401 (2018).
- [24] Bo Huang, Isabella Fritsche, Rianne S. Lous, Cosetta Baroni, Jook T. M. Walraven, Emil Kirilov, and Rudolf Grimm, “Breathing mode of a Bose-Einstein condensate repulsively interacting with a fermionic reservoir,” *Phys. Rev. A* **99**, 041602 (2019).
- [25] Luigi De Marco, Giacomo Valtolina, Kyle Matsuda, William G. Tobias, Jacob P. Covey, and Jun Ye, “A degenerate Fermi gas of polar molecules,” *Science* **363**, 853–856 (2019).
- [26] Zoe Z. Yan, Yiqi Ni, Carsten Robens, and Martin W. Zwierlein, “Bose polarons near quantum criticality,” *Science* **368**, 190–194 (2020).
- [27] Zhu-Xiong Ye, Li-Yang Xie, Zhen Guo, Xiao-Bin Ma, Gao-Ren Wang, Li You, and Meng Khoon Tey, “Double-degenerate Bose-Fermi mixture of strontium and lithium,” *Phys. Rev. A* **102**, 033307 (2020).
- [28] Hagai Edri, Boaz Raz, Noam Matzliah, Nir Davidson, and Roei Ozeri, “Observation of Spin-Spin Fermion-Mediated Interactions between Ultracold Bosons,” *Phys. Rev. Lett.* **124**, 163401 (2020).
- [29] Isabella Fritsche, Cosetta Baroni, Erich Dobler, Emil Kirilov, Bo Huang, Rudolf Grimm, Georg M. Bruun, and Pietro Massignan, “Stability and breakdown of Fermi polarons in a strongly interacting Fermi-Bose mixture,” *Phys. Rev. A* **103**, 053314 (2021).
- [30] Andreas Schindewolf, Roman Bause, Xing-Yan Chen, Marcel Duda, Tijs Karman, Immanuel Bloch, and Xin-Yu Luo, “Evaporation of microwave-shielded polar molecules to quantum degeneracy,” *Nature* **607**, 677–681 (2022).
- [31] Francesco Scazza, Matteo Zaccanti, Pietro Massignan, Meera M. Parish, and Jesper Levinsen, “Repulsive Fermi and Bose Polarons in Quantum Gases,” *Atoms* **10**, 55 (2022).
- [32] Xing-Yan Chen, Marcel Duda, Andreas Schindewolf, Roman Bause, Immanuel Bloch, and Xin-Yu Luo, “Suppression of Unitary Three-Body Loss in a Degenerate Bose-Fermi Mixture,” *Phys. Rev. Lett.* **128**, 153401 (2022).
- [33] Marcel Duda, Xing-Yan Chen, Andreas Schindewolf, Roman Bause, Jonas von Milczewski, Richard Schmidt, Immanuel Bloch, and Xin-Yu Luo, “Transition from a polaronic condensate to a degenerate Fermi gas of heteronuclear molecules,” *Nature Physics* **19**, 720 (2023).
- [34] Zoe Z. Yan, Yiqi Ni, Alexander Chuang, Pavel E. Dolgirev, Kushal Seetharam, Eugene Demler, Carsten Robens, and Martin Zwierlein, “Dissipationless flow in a Bose-Fermi mixture,” (2023), arXiv:2304.07663 [cond-mat.quant-gas].
- [35] Krutik Patel, Geyue Cai, Henry Ando, and Cheng Chin, “Sound Propagation in a Bose-Fermi Mixture: From Weak to Strong Interactions,” *Phys. Rev. Lett.* **131**, 083003 (2023).
- [36] B. J. DeSalvo, Krutik Patel, Geyue Cai, and Cheng Chin, “Observation of fermion-mediated interactions between bosonic atoms,” *Nature* **568**, 61 (2019).
- [37] Xin Shen, Nir Davidson, Georg M. Bruun, Mingyuan Sun, and Zhigang Wu, “Strongly Interacting Bose-Fermi Mixtures: Mediated Interaction, Phase Diagram, and Sound Propagation,” *Phys. Rev. Lett.* **132**, 033401 (2024).
- [38] Cosetta Baroni, Bo Huang, Isabella Fritsche, Erich Dobler, Gregor Anich, Emil Kirilov, Rudolf Grimm, Miguel A. Bastarrachea-Magnani, Pietro Massignan, and Georg M. Bruun, “Mediated interactions between Fermi polarons and the role of impurity quantum statistics,” *Nature Physics* **20**, 68–73 (2024).
- [39] Mateusz Bocheński, Jakub Dobosz, and Mariusz Semczuk, “Magnetic trapping of an ultracold ^{39}K - ^{40}K mixture with a versatile potassium laser system,” (2024), arXiv:2404.19670 [physics.atom-ph].
- [40] Jack B Muir, Jesper Levinsen, Stuart K Earl, Mitchell A Conway, Jared H Cole, Matthias Wurdack, Rishabh Mishra, David J Ing, Eliezer Estrecho, Yuerui Lu, *et al.*, “Interactions between Fermi polarons in monolayer WS₂,” *Nature Communications* **13**, 6164 (2022).
- [41] Ido Schwartz, Yuya Shimazaki, Clemens Kuhlenkamp, Kenji Watanabe, Takashi Taniguchi, Martin Kroner, and Ataç Imamoğlu, “Electrically tunable Fes-

- hbach resonances in twisted bilayer semiconductors,” *Science* **374**, 336–340 (2021).
- [42] Meinrad Sidler, Patrick Back, Ovidiu Cotlet, Ajit Srivastava, Thomas Fink, Martin Kroner, Eugene Demler, and Atac Imamoglu, “Fermi polaron-polaritons in charge-tunable atomically thin semiconductors,” *Nature Physics* **13**, 255–261 (2017).
- [43] Haifeng Kang, Jingwen Ma, Junyu Li, Xiang Zhang, and Xiaozhe Liu, “Exciton polaritons in emergent two-dimensional semiconductors,” *ACS nano* **17**, 24449–24467 (2023).
- [44] Gang Wang, Alexey Chernikov, Mikhail M. Glazov, Tony F. Heinz, Xavier Marie, Thierry Amand, and Bernhard Urbaszek, “Colloquium: Excitons in atomically thin transition metal dichalcogenides,” *Rev. Mod. Phys.* **90**, 021001 (2018).
- [45] Caterina Zerba, Clemens Kuhlenkamp, Ataç Imamoglu, and Michael Knap, “Realizing Topological Superconductivity in Tunable Bose-Fermi Mixtures with Transition Metal Dichalcogenide Heterostructures,” arXiv preprint arXiv:2310.10720 (2023).
- [46] Aleksii Julku, Jami J. Kinnunen, Arturo Camacho-Guardian, and Georg M. Bruun, “Light-induced topological superconductivity in transition metal dichalcogenide monolayers,” *Phys. Rev. B* **106**, 134510 (2022).
- [47] D. S. Petrov and G. V. Shlyapnikov, “Interatomic collisions in a tightly confined Bose gas,” *Phys. Rev. A* **64**, 012706 (2001).
- [48] Jesper Levinsen and Meera M. Parish, “Strongly Interacting Two-Dimensional Fermi Gases,” in *Annual Review of Cold Atoms and Molecules* (World Scientific, 2015) p. 1–75.
- [49] Elmar Haller, Manfred J. Mark, Russell Hart, Johann G. Danzl, Lukas Reichsöllner, Vladimir Melezhik, Peter Schmelcher, and Hanns-Christoph Nägerl, “Confinement-Induced Resonances in Low-Dimensional Quantum Systems,” *Phys. Rev. Lett.* **104**, 153203 (2010).
- [50] Giovanni Modugno, Giacomo Roati, Francesco Riboli, Francesca Ferlaino, Robert J. Brecha, and Massimo Inguscio, “Collapse of a degenerate Fermi gas,” *Science* **297**, 2240–2243 (2002).
- [51] B. Bazak and D. S. Petrov, “Stable p -Wave Resonant Two-Dimensional Fermi-Bose Dimers,” *Phys. Rev. Lett.* **121**, 263001 (2018).
- [52] Jami J. Kinnunen, Zhigang Wu, and Georg M. Bruun, “Induced p -Wave Pairing in Bose-Fermi Mixtures,” *Phys. Rev. Lett.* **121**, 253402 (2018).
- [53] Jonas von Milczewski, Xin Chen, Atac Imamoglu, and Richard Schmidt, “Superconductivity induced by strong electron-exciton coupling in doped atomically thin semiconductor heterostructures,” arXiv preprint arXiv:2310.10726 (2023).
- [54] V. Gurarie and L. Radzihovsky, “Resonantly paired fermionic superfluids,” *Annals of Physics* **322**, 2–119 (2007), january Special Issue 2007.
- [55] N. R. Cooper, J. Dalibard, and I. B. Spielman, “Topological bands for ultracold atoms,” *Rev. Mod. Phys.* **91**, 015005 (2019).
- [56] A Yu Kitaev, “Unpaired Majorana fermions in quantum wires,” *Physics-Uspekhi* **44**, 131 (2001).
- [57] A.Yu. Kitaev, “Fault-tolerant quantum computation by anyons,” *Annals of Physics* **303**, 2–30 (2003).
- [58] Biao Lian, Xiao-Qi Sun, Abolhassan Vaezi, Xiao-Liang Qi, and Shou-Cheng Zhang, “Topological quantum computation based on chiral Majorana fermions,” *PNAS* **115**, 10938–10942 (2018).
- [59] David Aasen, Michael Hell, Ryan V. Mishmash, Andrew Higginbotham, Jeroen Danon, Martin Leijnse, Thomas S. Jepsen, Joshua A. Folk, Charles M. Marcus, Karsten Flensberg, and Jason Alicea, “Milestones Toward Majorana-Based Quantum Computing,” *Phys. Rev. X* **6**, 031016 (2016).
- [60] Sankar Das Sarma, Michael Freedman, and Chetan Nayak, “Majorana zero modes and topological quantum computation,” *npj Quantum Information* **1**, 1–13 (2015).
- [61] Christina Knapp, Michael Beverland, Dmitry I. Pikulin, and Torsten Karzig, “Modeling noise and error correction for Majorana-based quantum computing,” *Quantum* **2**, 88 (2018).
- [62] Stephen Powell, Subir Sachdev, and Hans Peter Büchler, “Depletion of the Bose-Einstein condensate in Bose-Fermi mixtures,” *Phys. Rev. B* **72**, 024534 (2005).
- [63] D. B. M. Dickerscheid, D. van Oosten, E. J. Tillema, and H. T. C. Stoof, “Quantum Phases in a Resonantly Interacting Boson-Fermion Mixture,” *Phys. Rev. Lett.* **94**, 230404 (2005).
- [64] A. Storozhenko, P. Schuck, T. Suzuki, H. Yabu, and J. Dukelsky, “Boson-fermion pairing in a boson-fermion environment,” *Phys. Rev. A* **71**, 063617 (2005).
- [65] Alexander V. Avdeenkov, Daniele C. E. Bortolotti, and John L. Bohn, “Stability of fermionic Feshbach molecules in a Bose-Fermi mixture,” *Phys. Rev. A* **74**, 012709 (2006).
- [66] Lode Pollet, Matthias Troyer, Kris Van Houcke, and Stefan M. A. Rombouts, “Phase Diagram of Bose-Fermi Mixtures in One-Dimensional Optical Lattices,” *Phys. Rev. Lett.* **96**, 190402 (2006).
- [67] S. Röthel and A. Pelster, “Density and stability in ultracold dilute boson-fermion mixtures,” *The European Physical Journal B* **59**, 343–356 (2007).
- [68] X. Barillier-Pertuisel, S. Pittel, L. Pollet, and P. Schuck, “Boson-fermion pairing in Bose-Fermi mixtures on one-dimensional optical lattices,” *Phys. Rev. A* **77**, 012115 (2008).
- [69] Lode Pollet, Corinna Kollath, Ulrich Schollwöck, and Matthias Troyer, “Mixture of bosonic and spin-polarized fermionic atoms in an optical lattice,” *Phys. Rev. A* **77**, 023608 (2008).
- [70] D. C. E. Bortolotti, A. V. Avdeenkov, and J. L. Bohn, “Generalized mean-field approach to a resonant Bose-Fermi mixture,” *Phys. Rev. A* **78**, 063612 (2008).
- [71] Francesca M. Marchetti, Charles J. M. Mathy, David A. Huse, and Meera M. Parish, “Phase separation and collapse in Bose-Fermi mixtures with a Feshbach resonance,” *Phys. Rev. B* **78**, 134517 (2008).
- [72] Takayuki Watanabe, Toru Suzuki, and Peter Schuck, “Bose-Fermi pair correlations in attractively interacting Bose-Fermi atomic mixtures,” *Phys. Rev. A* **78**, 033601 (2008).
- [73] Elisa Fratini and Pierbiagio Pieri, “Pairing and condensation in a resonant Bose-Fermi mixture,” *Phys. Rev. A* **81**, 051605 (2010).
- [74] Zeng-Qiang Yu, Shizhong Zhang, and Hui Zhai, “Stability condition of a strongly interacting boson-fermion mixture across an interspecies Feshbach resonance,” *Phys. Rev. A* **83**, 041603 (2011).
- [75] Jun-Liang Song and Fei Zhou, “Anomalous dimers in quantum mixtures near broad resonances: Pauli blocking, Fermi surface dynamics, and implications,” *Phys. Rev. A* **84**, 013601 (2011).
- [76] D. Ludwig, S. Floerchinger, S. Moroz, and C. Wetterich, “Quantum phase transition in Bose-Fermi mixtures,” *Phys. Rev. A* **84**, 033629 (2011).
- [77] E. Fratini and P. Pieri, “Mass imbalance effect in resonant Bose-Fermi mixtures,” *Phys. Rev. A* **85**, 063618 (2012).
- [78] Arata Yamamoto and Tetsuo Hatsuda, “Quantum Monte Carlo simulation of three-dimensional Bose-Fermi mixtures,” *Phys. Rev. A* **86**, 043627 (2012).
- [79] Peter Anders, Philipp Werner, Matthias Troyer, Man-

- fred Sigrist, and Lode Pollet, “From the Cooper Problem to Canted Supersolids in Bose-Fermi Mixtures,” *Phys. Rev. Lett.* **109**, 206401 (2012).
- [80] G. Bertaina, E. Fratini, S. Giorgini, and P. Pieri, “Quantum Monte Carlo Study of a Resonant Bose-Fermi Mixture,” *Phys. Rev. Lett.* **110**, 115303 (2013).
- [81] E. Fratini and P. Pieri, “Single-particle spectral functions in the normal phase of a strongly attractive Bose-Fermi mixture,” *Phys. Rev. A* **88**, 013627 (2013).
- [82] T. Sogo, P. Schuck, and M. Urban, “Bose-Fermi pairs in a mixture and the Luttinger theorem within a Nozières-Schmitt-Rink-like approach,” *Phys. Rev. A* **88**, 023613 (2013).
- [83] Andrea Guidini, Gianluca Bertaina, Elisa Fratini, and Pierbiagio Pieri, “Bose-Fermi mixtures in the molecular limit,” *Phys. Rev. A* **89**, 023634 (2014).
- [84] L. Mathey, S.-W. Tsai, and A. H. Castro Neto, “Competing Types of Order in Two-Dimensional Bose-Fermi Mixtures,” *Phys. Rev. Lett.* **97**, 030601 (2006).
- [85] A. L. Subaşı, S. Sevinçli, P. Vignolo, and B. Tanatar, “Dimensional crossover in two-dimensional Bose-Fermi mixtures,” *Laser Physics* **20**, 683–693 (2010).
- [86] K. Noda, R. Peters, N. Kawakami, and Th Pruschke, “Quantum Phases of Bose-Fermi Mixtures in Optical Lattices,” *Journal of Physics: Conference Series* **273**, 012146 (2011).
- [87] Jonas von Milczewski, Félix Rose, and Richard Schmidt, “Functional-renormalization-group approach to strongly coupled Bose-Fermi mixtures in two dimensions,” *Phys. Rev. A* **105**, 013317 (2022).
- [88] Andrea Guidini, Gianluca Bertaina, Davide Emilio Galli, and Pierbiagio Pieri, “Condensed phase of Bose-Fermi mixtures with a pairing interaction,” *Phys. Rev. A* **91**, 023603 (2015).
- [89] P. C. Hohenberg, “Existence of Long-Range Order in One and Two Dimensions,” *Phys. Rev.* **158**, 383–386 (1967).
- [90] S. Simonucci, P. Pieri, and Giancarlo Strinati, “Broad vs. narrow Fano-Feshbach resonances in the BCS-BEC crossover with trapped Fermi atoms,” *Europhysics Letters (epL)* **69**, 713–718 (2005).
- [91] M. Schick, “Two-Dimensional System of Hard-Core Bosons,” *Phys. Rev. A* **3**, 1067–1073 (1971).
- [92] A. Fetter and J. D. Walecka, *Quantum Theory of Many-Particle Systems* (Dover Publications, 2003).
- [93] Jacopo D’Alberto, Lorenzo Cardarelli, Davide Emilio Galli, Gianluca Bertaina, and Pierbiagio Pieri, “Quantum Monte Carlo and perturbative study of two-dimensional Bose-Fermi mixtures,” *Phys. Rev. A* **109**, 053302 (2024).
- [94] H. Shi and A. Griffin, “Finite-temperature excitations in a dilute Bose-condensed gas,” *Physics Reports* **304**, 1–87 (1998).
- [95] V. N. Popov, *Functional integrals and collective excitations* (Cambridge University Press, Cambridge, 1987).
- [96] N. M. Hugenholtz and D. Pines, “Ground-State Energy and Excitation Spectrum of a System of Interacting Bosons,” *Phys. Rev.* **116**, 489–506 (1959).
- [97] Vuđtiwat Ngampruetikorn, Meera M. Parish, and Jesper Levinsen, “Three-body problem in a two-dimensional Fermi gas,” *Europhysics Letters* **102**, 13001 (2013).
- [98] Digvijay Kharga, Daisuke Inotani, Ryo Hanai, and Yoji Ohashi, “Single-Particle Excitations and Effects of Hetero-Pairing Fluctuations in a Bose-Fermi Mixture with a Feshbach Resonance,” *Journal of the Physical Society of Japan* **86**, 084301 (2017).
- [99] Koki Manabe, Daisuke Inotani, and Yoji Ohashi, “Single-particle properties of a strongly interacting Bose-Fermi mixture with mass and population imbalance,” *Phys. Rev. A* **100**, 063609 (2019).
- [100] Shina Tan, “Energetics of a strongly correlated Fermi gas,” *Annals of Physics* **323**, 2952–2970 (2008).
- [101] Shina Tan, “Large momentum part of a strongly correlated Fermi gas,” *Annals of Physics* **323**, 2971–2986 (2008).
- [102] Shina Tan, “Generalized virial theorem and pressure relation for a strongly correlated Fermi gas,” *Annals of Physics* **323**, 2987–2990 (2008).
- [103] Khalfan, H. Fayez and Byrd, R. H. and Schnabel, R. B., “A Theoretical and Experimental Study of the Symmetric Rank-One Update,” *SIAM Journal on Optimization* **3**, 1–24 (1993).
- [104] W. H. Press, S. A. Teukolski, W. T. Vetterling and B. P. Flannery, *Numerical recipes in Fortran 90: The art of Scientific Computing* (University Press, Cambridge, 1996).
- [105] Jonas Vlietinck, Jan Ryckebusch, and Kris Van Houcke, “Diagrammatic Monte Carlo study of the Fermi polaron in two dimensions,” *Phys. Rev. B* **89**, 085119 (2014).
- [106] Richard Schmidt, Tilman Enss, Ville Pietilä, and Eugene Demler, “Fermi polarons in two dimensions,” *Phys. Rev. A* **85**, 021602 (2012).
- [107] Pierbiagio Pieri, Andrea Perali, and Giancarlo Calvanese Strinati, “Enhanced paraconductivity-like fluctuations in the radiofrequency spectra of ultracold Fermi atoms,” *Nature Physics* **5**, 736–740 (2009).
- [108] R. Haussmann, M. Punk, and W. Zwerger, “Spectral functions and rf response of ultracold fermionic atoms,” *Phys. Rev. A* **80**, 063612 (2009).
- [109] Sascha Zöllner, G. M. Bruun, and C. J. Pethick, “Polarons and molecules in a two-dimensional Fermi gas,” *Phys. Rev. A* **83**, 021603 (2011).
- [110] Meera M. Parish, “Polaron-molecule transitions in a two-dimensional Fermi gas,” *Phys. Rev. A* **83**, 051603 (2011).
- [111] I. V. Brodsky, M. Yu. Kagan, A. V. Klaptsov, R. Combescot, and X. Leyronas, “Exact diagrammatic approach for dimer-dimer scattering and bound states of three and four resonantly interacting particles,” *Phys. Rev. A* **73**, 032724 (2006).
- [112] J. Levinsen and D. S. Petrov, “Atom-dimer and dimer-dimer scattering in fermionic mixtures near a narrow Feshbach resonance,” *The European Physical Journal D* **65**, 67–82 (2011).
- [113] P. Pieri and G. C. Strinati, “Trapped Fermions with Density Imbalance in the Bose-Einstein Condensate Limit,” *Phys. Rev. Lett.* **96**, 150404 (2006).
- [114] Gal Ness, Constantine Shkedorov, Yanay Florshaim, Oriana K. Diessel, Jonas von Milczewski, Richard Schmidt, and Yoav Sagi, “Observation of a Smooth Polaron-Molecule Transition in a Degenerate Fermi Gas,” *Phys. Rev. X* **10**, 041019 (2020).
- [115] G. V. Skorniakov and K. A. Ter-Martirosian, “Three body problem for short range forces. I. Scattering of low energy neutrons by deuterons,” *Soviet Phys. JETP* **4** (1957).